Cardiac fibroblasts mediate IL-17A–driven inflammatory dilated cardiomyopathy

Lei Wu,[1] SuFey Ong,[1] Monica V. Talor,[2] Jobert G. Barin,[2] G. Christian Baldeviano,[4] David A. Kass,[3] Djahida Bedja,[3] Hao Zhang,[1] Asfandyar Sheikh,[2] Joseph B. Margolick,[1] Yoichiro Iwakura,[5] Noel R. Rose,[1,2] and Daniela Čiháková [2]

[1]W. Harry Feinstone Department of Molecular Microbiology and Immunology, Johns Hopkins University Bloomberg School of Public Health, [2]Department of Pathology, and [3]Division of Cardiology, Department of Medicine, Johns Hopkins University School of Medicine, Baltimore, MD 21205
[4]Department of Parasitology, US Naval Medical Research Unit Six (NAMRU-6), Lima 34031, Peru
[5]Research Institute for Biomedical Sciences, Tokyo University of Science, Noda, Chiba 278-0022, Japan

Inflammatory dilated cardiomyopathy (DCMi) is a major cause of heart failure in individuals below the age of 40. We recently reported that IL-17A is required for the development of DCMi. We show a novel pathway connecting IL-17A, cardiac fibroblasts (CFs), GM-CSF, and heart-infiltrating myeloid cells with the pathogenesis of DCMi. Il17ra$^{-/-}$ mice were protected from DCMi, and this was associated with significantly diminished neutrophil and Ly6Chi monocyte/macrophage (MO/MΦ) cardiac infiltrates. Depletion of Ly6Chi MO/MΦ also protected mice from DCMi. Mechanistically, IL-17A stimulated CFs to produce key chemokines and cytokines that are critical downstream effectors in the recruitment and differentiation of myeloid cells. Moreover, IL-17A directs Ly6Chi MO/MΦ in trans toward a more proinflammatory phenotype via CF-derived GM-CSF. Collectively, this IL-17A–fibroblast–GM-CSF–MO/MΦ axis could provide a novel target for the treatment of DCMi and related inflammatory cardiac diseases.

CORRESPONDENCE
Daniela Čiháková:
dcihako1@jhmi.edu

Abbreviations used: α-SMA, α smooth muscle actin; BMDM, BM-derived macrophage; CF, cardiac fibroblast; CM, cardiomyocyte; DCMi, inflammatory dilated cardiomyopathy; EAM, experimental autoimmune myocarditis; EC, endothelial cell; IGF-1, insulin-like growth factor 1; LIF, leukemia inhibitory factor; MyHCα, cardiac myosin heavy chain α; qPCR, real-time quantitative PCR.

Inflammatory dilated cardiomyopathy (DCMi) is among the most common causes of noncongenital heart failure in individuals under the age of 40 (Dimas et al., 2009). There has been only limited success with symptomatic therapy in chronic DCMi patients, leaving cardiac transplantation the only cure for end stage heart failure secondary to DCMi (Pietra et al., 2012). Autoimmunity to heart tissue is often involved in the pathogenesis of DCMi (Čiháková and Rose, 2008; Cooper, 2009). In an effort to investigate the immunopathologic mechanism responsible for DCMi in humans, we have adopted a mouse model of experimental autoimmune myocarditis (EAM). EAM is induced by immunization of genetically susceptible BALB/c mice with a peptide derived from the cardiac myosin heavy chain α ($MyHC\alpha_{614-629}$). Immunized mice develop myocarditis characterized by inflammatory infiltration peaking about day 21, and subsequently progress to DCMi around day 40 to day 70, characterized by cardiac fibrosis and impairment of cardiac function (Čiháková et al., 2004).

EAM is a $CD4^+$ T helper cell–dependent disease (Smith and Allen, 1991, 1993). One of the $CD4^+$ T helper cell subsets, Th17 cells, has been observed to infiltrate the heart during EAM (Baldeviano et al., 2010), and has been reported to be critical in autoimmunity (Korn et al., 2009). Furthermore, patients with DCMi have increased numbers of Th17 cells in their blood and an elevated level of Th17 cytokines in serum, suggesting that Th17 cells are involved in the pathogenesis of DCMi (Ding et al., 2010; Yuan et al., 2010). When we examined whether the hallmark Th17 cytokine, IL-17A, drives the pathogenesis of myocarditis, we discovered that *Il17a*$^{-/-}$ mice were completely protected from the development of DCMi, although they had myocardial inflammation comparable in overall severity to WT controls (Baldeviano et al., 2010). Thus, IL-17A is dispensable for early

The Rockefeller University Press $30.00
J. Exp. Med. 2014 Vol. 211 No. 7 1449-1464
www.jem.org/cgi/doi/10.1084/jem.20132126

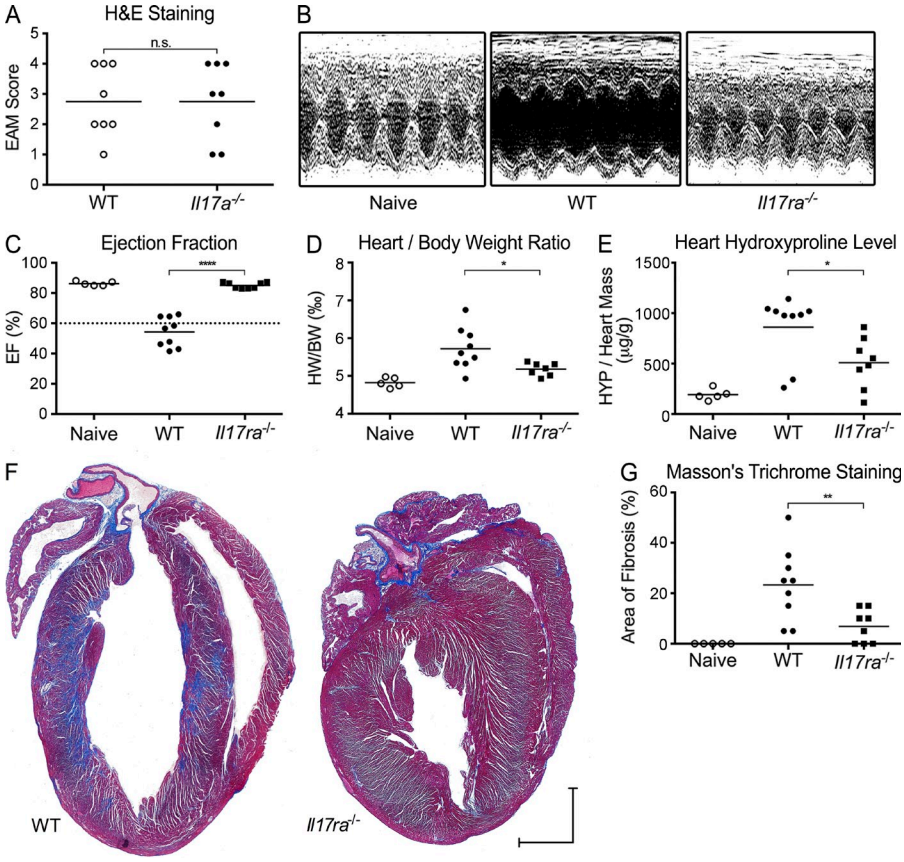

Figure 1. *Il17ra*$^{-/-}$ mice are protected from DCMi. EAM and DCMi were induced in WT and *Il17ra*$^{-/-}$ mice. On days 0 and 7, mice received s.c. immunizations of 100 µg MyHC$\alpha_{614-629}$ peptide emulsified in CFA supplemented to 5 mg/ml of heat-killed *M. tb* strain H37Ra. On day 0, mice also received 500 ng pertussis toxin i.p. (A) Mice were sacrificed 21 d after immunization. EAM was scored using H&E staining as described in Materials and methods. Data are representative of 3 independent experiments. Data points represent individual mice. Horizontal bars represent mean. Data are analyzed by Mann-Whitney *U* test. n.s. = not significant. (B–G) 63 d after immunization, naive and immunized mice underwent echocardiography and were sacrificed. (B) Representative M-Mode echocardiography of naive, WT, and *Il17ra*$^{-/-}$ mice. (C) Ejection fraction (%) of naive, WT, and *Il17ra*$^{-/-}$ mice by echocardiography. Dotted line marks 60%, the threshold for severe DCMi. (D) Heart weight/body weight ratio (‰). (E) Cardiac hydroxyproline assay normalized to heart weight. (F) Representative histopathology of *Il17ra*$^{-/-}$ and WT mice hearts showing Masson's trichrome blue staining. Fibrotic tissue was stained blue. Bars, 1 mm. (G) Cardiac fibrosis in *Il17ra*$^{-/-}$ and WT mice scored using Masson's trichrome blue staining. (B–G) Data are representative of 3 independent experiments. Data points represent individual mice. Horizontal bars represent mean. Data were analyzed by one-way ANOVA followed by Tukey's post-test. *, $P < 0.05$; **, $P < 0.01$; ****, $P < 0.0001$.

stage myocarditis but required for the progression to DCMi. These results indicated a critical role of IL-17A in driving cardiac damage and fibrosis during the development of DCMi. Similar profibrotic functions of IL-17A have been reported in cirrhosis (Lan et al., 2009) and fibrotic lung injury (Wilson et al., 2010) models.

Monocytes (MOs) and macrophages (MΦs) are key effector cells during inflammatory processes (Gordon and Taylor, 2005) including myocarditis and DCMi. MO/MΦs comprise about half of all heart-infiltrating inflammatory cells at the peak of EAM and play important roles in the pathogenesis (Čiháková et al., 2008; Barin et al., 2012). Monocytes arise from hematopoietic stem cells and form distinct subpopulations. In mouse, the two monocyte subsets, CCR2^{hi}CX3CR1^{lo}Ly6C^{hi} and CCR2^{lo}CX3CR1^{hi}Ly6C^{lo} monocytes, infiltrate sites of inflammation responding to different chemokine signals and differentiate into inflammatory MΦs guided by local cytokine signals (Gordon and Taylor, 2005; Shi and Pamer, 2011). The balance between MO/MΦ subsets and their differentiation is critical in determining the pathogenic outcome in immune responses (Wynn et al., 2013). In this paper, while examining the pathogenic mechanisms of IL-17A–dependent DCMi, we describe a novel immunological pathway connecting IL-17A with MO/MΦs that drives DCMi development.

RESULTS

IL-17A/IL-17RA signaling is required for the development of DCMi

We previously demonstrated that *Il17a*$^{-/-}$ mice are susceptible to EAM but are protected from DCMi (Baldeviano et al., 2010). To investigate the downstream functions of IL-17A in the development of DCMi, we first excluded the possibility that other IL-17 family cytokines signaling though the IL-17 receptor contributed to the DCMi phenotype by comparing disease in *Il17ra*$^{-/-}$ and *Il17a*$^{-/-}$ mice. Similar to *Il17a*$^{-/-}$ mice, *Il17ra*$^{-/-}$ mice were fully protected from DCMi after immunization with myocarditogenic peptide MyHC$\alpha_{614-629}$, although they developed myocarditis histologically comparable to WT controls (Fig. 1 A). *Il17ra*$^{-/-}$ mice retained normal heart function and were protected from ventricular dilation (Fig. 1, B and C). In addition, *Il17ra*$^{-/-}$ mice developed limited cardiac enlargement (Fig. 1 D) and fibrosis, whereas WT mice hearts had significant fibrosis as determined by hydroxyproline

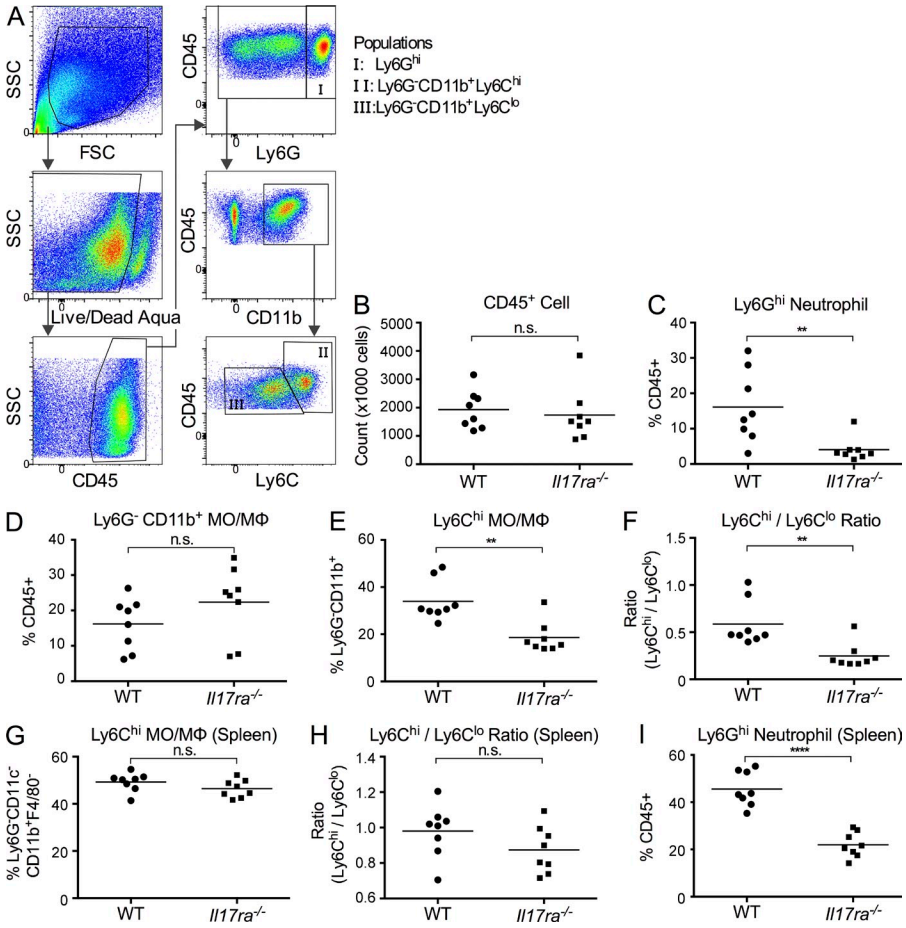

Figure 2. IL-17RA deficiency alters the composition of heart-infiltrating cells. EAM and DCMi were induced in WT and *Il17ra*$^{-/-}$ mice. Mice were sacrificed 21 d after immunization. (A–F) The composition of heart-infiltrating inflammatory cells was analyzed by flow cytometry. (A) Representative gating of heart-infiltrating myeloid cells. (B) Total cell number of intracardiac CD45$^+$ leukocytes in WT and *Il17ra*$^{-/-}$ mice. (C) Intracardiac Ly6G^{hi} neutrophils as a proportion of total CD45$^+$ leukocytes. (D) Intracardiac Ly6G$^-$CD11b$^+$ MO/MΦs as a proportion of total CD45$^+$ leukocytes. (E) Ly6C^{hi} MO/MΦs as a proportion of Ly6G$^-$CD11b$^+$ population. (F) Ly6C^{hi} to Ly6C^{lo} MO/MΦ ratio. (G–I) The composition of splenocytes was analyzed by flow cytometry with gating similar to A. (G) Ly6C^{hi} monocytes as a proportion of total Ly6G$^-$CD11c$^-$CD11b$^+$F4/80$^-$ population in the spleen. (H) Ly6C^{hi} to Ly6C^{lo} monocyte ratio in the spleen. (I) Ly6G^{hi} neutrophils as a proportion of total CD45$^+$ leukocytes in the spleen. For bar graphs, data are representative of 3 independent experiments. Data points represent individual mice. Horizontal bars represent mean. Data are analyzed by unpaired two-tailed Student's *t* test. **, $P < 0.01$; ****, $P < 0.0001$; n.s. = not significant.

assay (Fig. 1 E) and Masson's trichrome staining (Fig. 1, F and G). Thus, we established that the IL-17A/IL-17RA signaling pathway is required for the development of DCMi. Moreover, because *Il17ra*$^{-/-}$ mice had disease similar to *Il17a*$^{-/-}$ mice, it is unlikely that other cytokines of the IL-17 family are critical in the pathogenesis of DCMi.

IL-17RA deficiency alters the composition of heart-infiltrating myeloid populations during EAM

Histopathologic and flow cytometric analyses (Fig. 2 A) revealed that *Il17ra*$^{-/-}$ mice had a similar degree of inflammation and quantitatively comparable numbers of heart-infiltrating CD45$^+$ cells as WT controls (Fig. 2 B). There was no significant difference in the percentages of infiltrating CD4$^+$ T cells or SiglecF$^+$ eosinophils (unpublished data). However, IL-17RA deficiency led to profound changes in the composition of infiltrating myeloid cells. Specifically, *Il17ra*$^{-/-}$ mice had significantly diminished Ly6G^{hi} neutrophil infiltration in their hearts (Fig. 2 C). Moreover, even though the proportion of total Ly6G$^-$CD11b$^+$ monocyte/macrophage (MO/MΦ) population in CD45$^+$ cells was comparable (Fig. 2 D), *Il17ra*$^{-/-}$ mice had significantly lower levels of Ly6C^{hi} population and higher levels of Ly6C^{lo} population within the Ly6G$^-$CD11b$^+$ MO/MΦ compartment (Fig. 2, E and F). Importantly, this shift in MO/MΦ populations was restricted to the heart, as the levels of Ly6C^{hi} and Ly6C^{lo} monocytes in the spleen were comparable between WT and *Il17ra*$^{-/-}$ mice (Fig. 2, G and H). This was dissimilar to the reduction in cardiac infiltration of Ly6G^{hi} neutrophils, which was also detected in the spleen (Fig. 2 I). The specificity of the difference in the ratio of Ly6C^{hi} to Ly6C^{lo} MO/MΦs in the heart indicates that local but not systemic signals drive this change. In summary, protection from DCMi in *Il17ra*$^{-/-}$ mice is closely associated with the composition of myeloid populations in the heart, particularly with a significant diminution of neutrophils and Ly6C^{hi} MO/MΦs.

Intracardiac Ly6C^{hi} MO/MΦs have proinflammatory and profibrotic phenotype, whereas Ly6C^{lo} MO/MΦs up-regulate insulin-like growth factor 1 (IGF-1) and MMP production

The striking decrease in the ratio of Ly6C^{hi} to Ly6C^{lo} MO/MΦs in the absence of IL-17RA signaling led us to examine the contribution of these cell subsets to cardiac damage and fibrosis during DCMi development. Using FACS, we isolated CD45$^+$Ly6G$^-$CD11b$^+$Ly6C^{hi} and CD45$^+$Ly6G$^-$CD11b$^+$Ly6C^{lo} MO/MΦs separately from WT mouse hearts at the peak of inflammation on day 21. Transcriptome profiles were generated by real-time quantitative PCR (qPCR) analysis of these two populations (Fig. 3 A and Table 1).

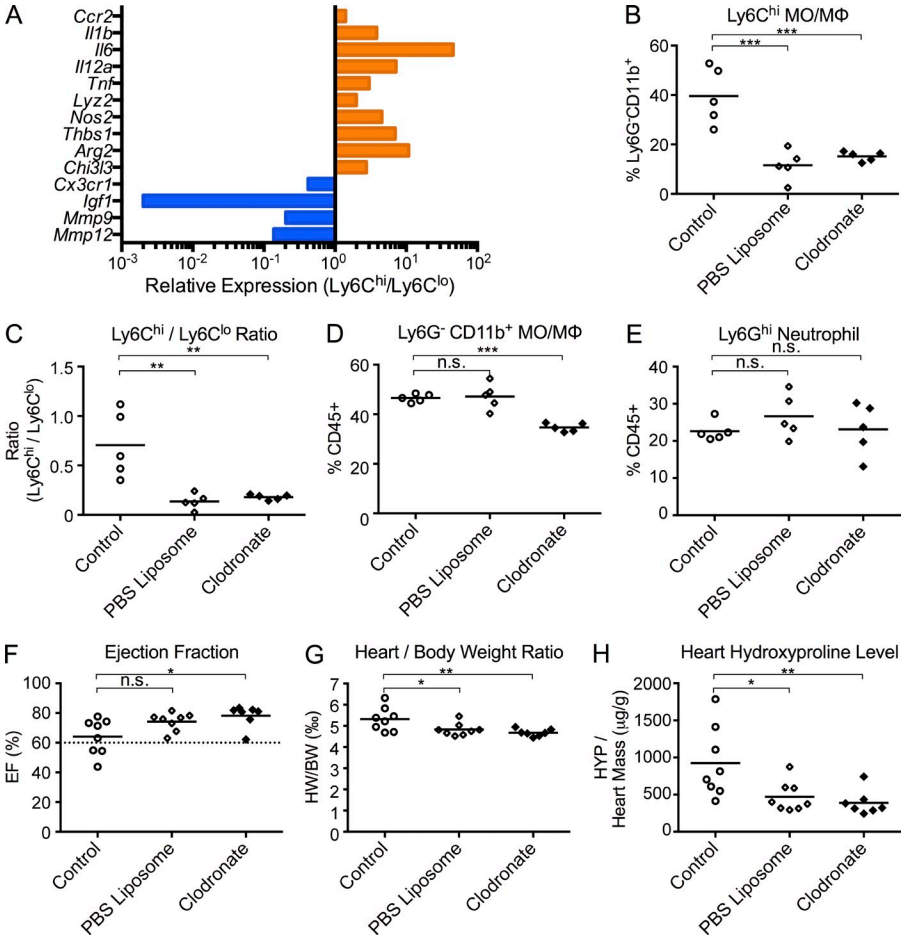

Figure 3. Transcriptomes and functions of intracardiac Ly6C^{hi} and Ly6C^{lo} MO/MΦs. (A) EAM and DCMi were induced in WT mice. Mice were sacrificed 21 d after immunization. Ly6G$^-$CD11b$^+$Ly6C^{hi} (Ly6C^{hi}) and Ly6G$^-$CD11b$^+$Ly6C^{lo} (Ly6C^{lo}) MO/MΦ populations were isolated from mouse hearts by FACS. mRNA levels were determined by qPCR, normalized to housekeeping gene *Hprt*. Detailed data are shown in Table 1. For each individual gene, the ratio of its expression in Ly6C^{hi} population versus that in Ly6C^{lo} was calculated and plotted in log scale. Ratio greater than one indicates the gene was up-regulated in Ly6C^{hi} MO/MΦs (orange), and ratio smaller than one indicates that the gene was up-regulated in Ly6C^{lo} MO/MΦs (blue). Data are representative of 2 independent experiments. (B–E) EAM and DCMi were induced in WT mice. On days 14, 16, 18, and 20, mice were injected i.v. with 250 µl PBS (control), PBS-loaded liposome (PBS liposome), or clodronate-loaded liposome (clodronate). Mice were sacrificed 21 d after immunization. The composition of heart-infiltrating cells was analyzed by flow cytometry. Data are representative of 2 independent experiments. (B) Ly6C^{hi} MO/MΦs as a proportion of Ly6G$^-$CD11b$^+$ population. (C) Ly6C^{hi} to Ly6C^{lo} MO/MΦ ratio. (D) Intracardiac Ly6G$^-$CD11b$^+$ MO/MΦs as a proportion of total CD45$^+$ leukocytes. (E) Intracardiac Ly6G^{hi} neutrophils as a proportion of total CD45$^+$ leukocytes. (F–H) EAM and DCMi were induced in WT mice. From days 14 to 35, mice were injected i.v. every other day with 250 µl PBS (control), PBS-loaded liposome (PBS liposome), or clodronate-loaded liposome (clodronate). 63 d after immunization, mice underwent echocardiography and were sacrificed. Data are representative of 2 independent experiments. (F) Ejection fraction (%) by echocardiography. Dash line marks 60%, the threshold for severe DCMi. (G) Heart weight/body weight ratio (‰). (H) Cardiac hydroxyproline assay normalized to heart weight. For bar graphs, data points represent individual mice. Horizontal bars represent mean. Data were analyzed by one-way ANOVA followed by Tukey's post-test. *, $P < 0.05$; **, $P < 0.01$; ***, $P < 0.001$; n.s. = not significant.

Ly6C^{hi} MO/MΦs were characterized by higher *Ccr2* expression. Compared with the Ly6C^{lo} population, Ly6C^{hi} MO/MΦs produced higher levels of several proinflammatory cytokines and enzymes (*Il1b*, *Il6*, *Il12a*, *Tnf*, and *Nos2*). In addition, Ly6C^{hi} MO/MΦs up-regulated thrombospondin-1 (*Thbs1*), which activates latent TGF-β trapped in the extracellular matrix (ECM) and initiates TGF-β–dependent fibrosis pathways (Frangogiannis, 2012). Ly6C^{hi} MO/MΦs also produced more arginase 2 (*Arg2*) and YM1 (*Chi3l3*), which are traditionally associated with M2 tissue repair macrophages, indicating that the classic M1/M2 dichotomy does not perfectly fit with Ly6C^{hi}/Ly6C^{lo} MO/MΦ phenotypes in the cardiac inflammation scenario during EAM and DCMi. Conversely, Ly6C^{lo} MO/MΦs are characterized by greater expression of *Cx3cr1*, and they produced higher levels of matrix metalloproteinases (*Mmp9* and *Mmp12*) and *Igf1* (Fig. 3 A). These molecules have been implicated in protecting against tissue fibrosis by breaking down excessive ECM (Ramachandran et al., 2012) as well as by other mechanisms (Bessich et al., 2013).

To summarize, heart-infiltrating Ly6C^{hi} MO/MΦs display a proinflammatory and profibrotic phenotype indicating a pathogenic role, whereas Ly6C^{lo} MO/MΦs produced a high level of MMPs and IGF-1 suggesting a protective role. Therefore, *Il17ra*$^{-/-}$ mice had significantly less inflammatory monocytic infiltration in their hearts during the peak of inflammation, which helps to explain their resistance to DCMi.

Ly6C^{hi} MO/MΦs aggravate DCMi

To test the hypothesis that Ly6C^{hi} MO/MΦs directly promote DCMi, we manipulated the balance of Ly6C^{hi} and Ly6C^{lo} MO/MΦs in vivo using two previously published methods. First, we injected mice with clodronate-loaded liposomes, which have been shown to induce apoptosis in MO/MΦs (van Rooijen et al., 1996). Second, we injected mice with PBS-loaded liposomes, which have been reported to induce a phenotypic switch from Ly6C^{hi} to Ly6C^{lo} MO/MΦs through the phagocytosis of the liposomes (Ramachandran et al., 2012).

Table 1. Transcriptomes of intracardiac Ly6C^{hi} and Ly6C^{lo} MO/MΦs

Gene	Ly6C^{hi} MO/MΦ	95% CI	Ly6C^{lo} MO/MΦ	95% CI	P-value	Ly6C^{hi}/Ly6C^{lo} Ratio
	GeoMean		GeoMean			
Ccr2	2.97^{+00}	(2.49^{+00}, 3.45^{+00})	2.10^{+00}	(1.94^{+00}, 2.26^{+00})	0.0270	1.41
Il1b	7.54^{+01}	(6.40^{+01}, 8.68^{+01})	1.97^{+01}	(1.48^{+01}, 2.45^{+01})	0.0009	3.84
Il6	1.80^{+00}	(1.14^{+00}, 2.47^{+00})	2.51^{-01}	(1.58^{-01}, 3.43^{-01})	0.0093	7.19
Il12a	7.55^{-02}	(4.03^{-02}, 1.11^{-01})	1.65^{-03}	(0, 1.03^{-02})	0.0170	45.78
Tnf	2.36^{+00}	(1.39^{+00}, 3.33^{+00})	7.83^{-01}	(3.67^{-01}, 1.20^{+00})	0.0392	3.02
Lyz2	1.42^{+02}	(9.97^{+01}, 1.85^{+02})	7.17^{+01}	(5.03^{+01}, 9.30^{+01})	0.0411	1.99
Nos2	7.13^{-02}	(3.44^{-02}, 1.08^{-01})	1.57^{-02}	(1.05^{-02}, 2.09^{-02})	0.0341	4.54
Thbs1	2.68^{+00}	(1.39^{+00}, 3.98^{+00})	3.83^{-01}	(3.25^{-01}, 4.42^{-01})	0.0199	7.00
Arg2	1.33^{+00}	(1.09^{+00}, 1.58^{+00})	4.83^{-01}	(1.93^{-01}, 7.73^{-01})	0.0136	2.76
Chi3l3	6.80^{-01}	(4.10^{-01}, 9.50^{-01})	6.28^{-02}	(1.51^{-02}, 1.11^{-01})	0.0105	10.83
Cx3cr1	1.00^{+00}	(3.84^{-01}, 1.63^{+00})	2.39^{+00}	(2.09^{+00}, 2.70^{+00})	0.0212	0.419
Igf1	6.10^{-05}	(8.28^{-06}, 1.14^{-04})	2.66^{-02}	(1.15^{-02}, 4.16^{-02})	0.0207	0.002
Mmp9	6.12^{-03}	(0, 1.49^{-02})	3.01^{-02}	(2.34^{-02}, 3.68^{-02})	0.0194	0.203
Mmp12	1.57^{-01}	(0, 3.59^{-01})	1.15^{+00}	(7.77^{-01}, 1.51^{+00})	0.0103	0.137

EAM and DCMi were induced in WT mice. Mice were sacrificed 21 d after immunization. Ly6G$^-$CD11b$^+$Ly6C^{hi} (Ly6C^{hi}) and Ly6G$^-$CD11b$^+$Ly6C^{lo} (Ly6C^{lo}) MO/MΦ populations were isolated from mouse hearts by FACS. mRNA levels were determined by real-time qPCR and normalized to housekeeping gene *Hprt*. Data are representative of 2 independent experiments. Geometric mean of 3 replicates and 95% confidence interval (95% CI) are shown. The ratios of the mRNA levels in Ly6C^{hi} population to Ly6C^{lo} population are calculated. Data are analyzed by unpaired two-tailed Student's *t* test.

To assess how these treatments affect the myocarditis phase of EAM, we injected PBS-loaded or clodronate-loaded liposomes on days 14, 16, 18, and 20 of EAM, and sacrificed the mice on day 21. PBS-loaded liposomes significantly reduced the proportion of Ly6C^{hi} MO/MΦs among all Ly6G$^-$CD11b$^+$ MO/MΦs (Fig. 3 B) and dramatically lowered the ratio of Ly6C^{hi} to Ly6C^{lo} MO/MΦs (Fig. 3 C), while not affecting the total number of Ly6G$^-$CD11b$^+$ MO/MΦs among heart-infiltrating CD45$^+$ cells (Fig. 3 D). Clodronate-loaded liposomes, however, significantly decreased the total number of Ly6G$^-$CD11b$^+$ MO/MΦs in the heart (Fig. 3 D), but also disproportionately reduced the proportion of Ly6C^{hi} MO/MΦs among MO/MΦs (Fig. 3 B) and lowered the Ly6C^{hi} to Ly6C^{lo} MO/MΦ ratio (Fig. 3 C). Both PBS-loaded and clodronate-loaded liposome treatments had no significant effect on the severity of EAM on day 21 (not depicted), and the levels of Ly6G^{hi} neutrophil infiltration in the heart were not affected (Fig. 3 E).

We next administered PBS- or clodronate-loaded liposomes intravenously every other day from days 14 to 35 of EAM, through the peak of cardiac inflammation, and assessed the severity of DCMi at day 63. Clodronate-loaded liposomes protected mice from the deterioration of cardiac function (Fig. 3 F). PBS-loaded liposomes also showed promising effects, as none of the PBS-loaded liposome-treated mice developed severe DCMi defined by an ejection fraction <60% (Fig. 3 F). Furthermore, mice treated with PBS-loaded or clodronate-loaded liposomes had significantly reduced cardiac enlargement (Fig. 3 G) and fibrosis (Fig. 3 H). These results illustrate that although Ly6C^{hi} MO/MΦs are not essential in the pathogenesis of acute myocarditis, they play critical roles in cardiac fibrosis and the development of DCMi.

IL-17A/IL-17RA signaling to cardiac-resident cells is required for the development of DCMi

Protection of *Il17ra*$^{-/-}$ mice against DCMi is associated with significant diminution in neutrophil and Ly6C^{hi} monocyte infiltration. In the inflamed heart, IL-17A receptors are expressed by both infiltrating hematopoietic cells (Gaffen, 2009) and cardiac-resident cells (Fig. 4 A). To determine whether IL-17A drives DCMi by directly signaling to infiltrating hematopoietic cells or indirectly through cardiac-resident cells, we generated BM chimeras. WT or *Il17ra*$^{-/-}$ BMs were transferred into lethally irradiated *Il17ra*$^{-/-}$ or WT recipients to generate BM chimeras with IL-17RA signaling ablated in either hematopoietic or nonhematopoietic compartments (Fig. 4 B). Syngeneic transfers were performed as controls to exclude the effects of the BM reconstruction itself. Chimeras lacking IL-17RA on their cardiac-resident cells were protected from DCMi, regardless of the genotype of their BM donors. Their hearts retained normal function (Fig. 4 C) with lower levels of collagen deposition in their hearts (Fig. 4 D). Two-way ANOVA (genotype of recipients vs. genotype of donors) confirmed the genotype of recipient mice as the primary source of variance. Chimeras lacking IL-17RA signaling in their hematopoietic compartment showed partially mitigated DCMi compared with WT syngeneic transfer controls; however, they were not fully protected from DCMi as the chimeras with *Il17ra*$^{-/-}$ BMs (Fig. 4, C and D), suggesting

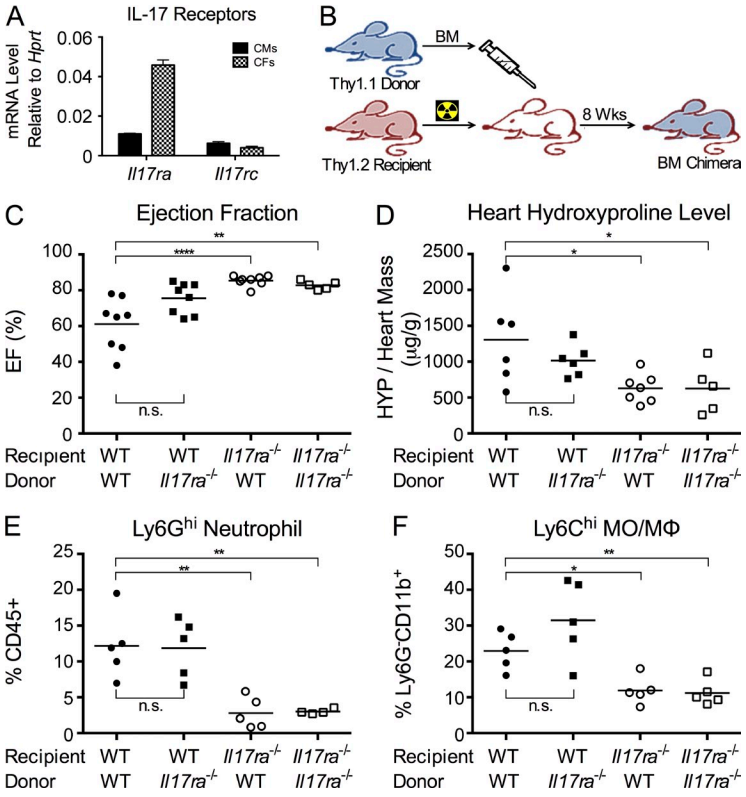

Figure 4. IL-17RA signaling to cardiac-resident cells is required for the development of DCMi. (A) Primary adult mouse CMs and CFs were isolated from naive WT mice. mRNA of *Il17ra* and *Il17rc* were detected by real-time qPCR. Data are representative of 2 independent experiments. Data are shown as mean + SEM of three replicates. (B) Schematic of the generation of BM chimeras. BMs were transferred from WT or *Il17ra*$^{-/-}$ Thy1.1 donor into lethally irradiated *Il17ra*$^{-/-}$ or WT Thy1.2 recipients. EAM and DCMi were induced 8 wk after transfer. (C and D) 63 d after immunization, chimeric mice underwent echocardiography and were sacrificed. Data are representative of 4 independent experiments. (C) Ejection fraction (%) of BM chimeras with depicted genotypes. (D) Cardiac hydroxyproline assay normalized to heart weight. (E and F) 21 d after immunization, chimeric mice were sacrificed, and their heart-infiltrating cells were analyzed by flow cytometry. Data are representative of 3 independent experiments. (E) Intracardiac Ly6G^{hi} neutrophil as a proportion of CD45^{+} leukocytes in BM chimeras with depicted genotype. (F) Ly6C^{hi} MO/MΦs as a proportion of Ly6G^{-}CD11b^{+} population. For bar graphs, data points represent individual mice. Horizontal bars represent mean. Data are analyzed by two-way ANOVA (genotype of donor vs. genotype of recipient) followed by Tukey's post-test. *, P < 0.05; **, P < 0.01; ****, P < 0.0001; n.s. = not significant.

that IL-17RA signaling to hematopoietic cells is dispensable in the development of DCMi.

IL-17A/IL-17RA signaling to cardiac-resident cells results in neutrophil and Ly6C^{hi} MO/MΦ-rich infiltrate

We observed that the protection from DCMi in *Il17ra*$^{-/-}$ mice was associated with diminished neutrophils and Ly6C^{hi} monocyte infiltration (Fig. 2, C and E). To examine if this alteration in the cardiac infiltrate is due to IL-17A signaling to cardiac-resident cells, we analyzed the composition of heart-infiltrating cells in chimeras at the peak of inflammation on day 21. Flow cytometric analysis showed that lack of IL-17RA signaling in nonhematopoietic cardiac-residents cells diminished neutrophil and Ly6C^{hi} MO/MΦ infiltration, mirroring our finding in *Il17ra*$^{-/-}$ mice hearts (Fig. 4, E and F). Thus, IL-17RA signaling in cardiac-resident cells is mainly responsible for regulating the composition of myeloid cells in the cardiac infiltrate, and is required for cardiac fibrosis during DCMi pathogenesis.

IL-17A fails to induce apoptosis in adult mouse cardiomyocytes (CMs)

Having established that IL-17A signaling to cardiac-resident cells is essential in driving cardiac damage and fibrosis during DCMi, we sought to identify the specific cell target of IL-17A. We isolated primary CMs from adult WT mice and stimulated them with recombinant IL-17A (rIL-17A) in vitro. After 24 h, we assessed CM viability and morphology. A recent study found that IL-17A was able to induce apoptosis in neonatal CMs in vitro, and the authors suggested that this

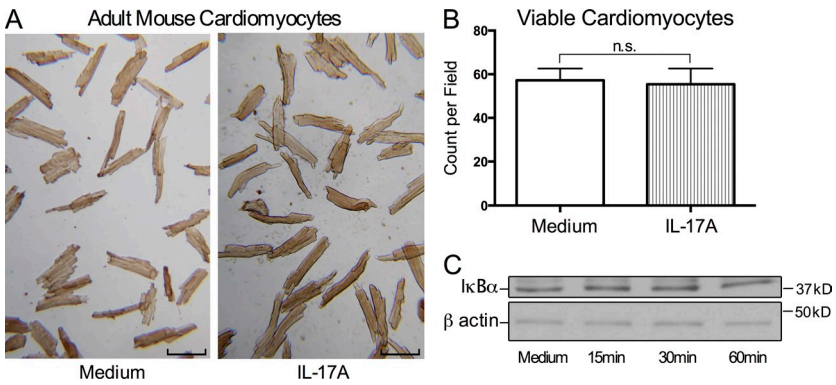

Figure 5. IL-17A has no significant effects on adult mouse CMs in vitro. (A and B) Primary adult mouse CMs were cultured with or without 100 ng/ml rIL-17A for 24 h. Data are representative of 3 independent experiments. (A) Bright field microscopy showed cell morphology and viability of rIL-17A–treated and control CMs. Bars, 100 μm. (B) Viable CMs were counted in 5 different fields. Data are shown as mean + SEM and analyzed by unpaired two-tailed Student's *t* test. n.s. = not significant. (C) Primary adult CMs were stimulated with 100 ng/ml rIL-17A for 15, 30, or 60 min. Cells were lysed and probed by Western blotting for IκBα and β actin as control. Data are representative of 2 independent experiments.

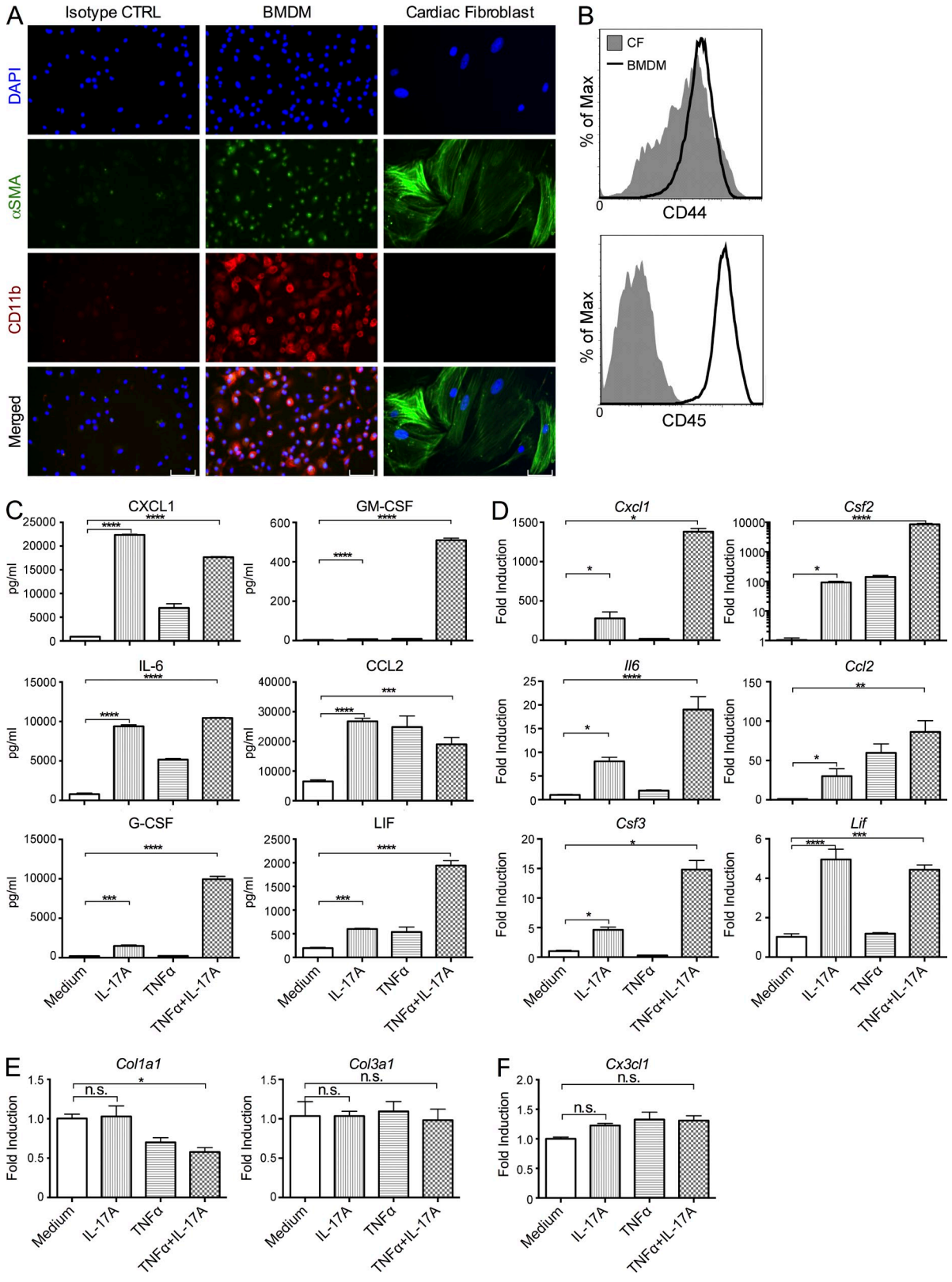

Figure 6. IL-17A stimulates the production of myeloid chemokines and cytokines in adult CFs in vitro. (A) Primary adult mouse CFs from naive WT mice and BMDMs were cultured on chamber slides. Immunofluorescence microscopy shows staining for α-SMA (green) and CD11b (red). BMDMs were stained with isotype-matched antibodies as isotype control. Data are representative of 2 independent experiments. Bars, 100 µM. (B) The expression of surface markers CD44 and CD45 in CF (filled) and BMDM (open) cultures were analyzed by flow cytometry. Levels of expression on all 7-AAD–negative

effect contributed to CM death during myocardial infarction in adults (Liao et al., 2012). However, adult CMs stimulated with rIL-17A retained their viability and morphology when compared with unstimulated CM culture (Fig. 5, A and B). Thus, IL-17A does not induce apoptosis in primary adult CMs in vitro. In addition, qPCR assay of CM mRNA did not detect any induction of classic IL-17A targets, including *Il6* and *Cxcl1* (unpublished data). Previous studies suggested that TNF synergizes with IL-17A by stabilizing mRNA of IL-17A targets (Ruddy et al., 2004). However, addition of rTNF to the culture did not induce activation of IL-17A targets either (unpublished data). IL-17A signals through the classical NF-κB pathway, which requires the degradation of NF-κB inhibitor IκBα (Gaffen, 2009). However, Western blotting showed that IL-17A failed to induce IκBα degradation in adult CMs (Fig. 5 C). To summarize, IL-17A does not appear to have any significant effects on adult CMs in vitro, indicating that CMs are not the primary IL-17A target during DCMi.

IL-17A induces myeloid chemokines and cytokines production from cardiac fibroblasts (CFs)

Next, we assessed the effect of IL-17A signaling to CFs. We isolated primary CFs from WT adult mice and tested the purity of CF culture to rule out the possibility of contamination by macrophages and other cells. BM-derived macrophages (BMDMs) were used as a positive control. First, using immunofluorescence microscopy, we found that cells in our CF culture expressed α smooth muscle actin (α-SMA) but not myeloid marker CD11b (Fig. 6 A). Second, by flow cytometry, we did not detect any $CD45^+$ leukocytes in our culture contaminating the $CD44^+$ CF population (Fig. 6 B). Third, by qPCR, we detected the expression of fibroblast-specific genes *Agtr1a* (angiotensin II receptor, type 1a) and *Ddr2* (discoidin domain receptor family member 2) in CF culture, but not genes expressed by myeloid cells, including *Ccr2*, *Cx3cr1*, *Mpo*, or *Pgcd1lg2* (PD-L2; unpublished data). Based on the sensitivity of qPCR assay and the number of cells in the culture, macrophage contamination in CF culture, if any, is extremely low.

To assess the effect of IL-17A on CFs, we isolated primary CFs from adult WT mice and stimulated with IL-17A for 24 h. IL-17A was able to induce the production of CXCL1, CCL2, GM-CSF, G-CSF, IL-6, and leukemia inhibitory factor (LIF; Fig. 6 C), but not IL-1β, IL-33, TNF, TGF-β, CCL8, and CCL11 (not depicted). Addition of TNF further enhanced the stimulatory effects of IL-17A (Fig. 6 C). Interrogation of mRNA levels by qPCR confirmed these effects (Fig. 6 D). However, IL-17A failed to directly stimulate the production of collagen (Fig. 6 E) or *Cx3cl1* (Fig. 6 F) in CFs, indicating that more complex mechanisms were involved in regulating fibrosis and the accumulation of $Ly6C^{lo}$ MO/MΦs in *Il17ra*$^{-/-}$ hearts during IL-17A–driven DCMi.

To confirm these results in vivo, we next isolated $CD45^-CD34^+CD146^+CD44^{hi}CD31^-$ CFs from the hearts of immunized WT and *Il17ra*$^{-/-}$ mice by FACS (Fig. 7 A). qPCR analysis showed that CFs from *Il17ra*$^{-/-}$ mice expressed significantly lower levels of *Cxcl1*, *Csf2*, *Csf3*, and *Il6* compared with CFs from WT mice (Fig. 7 B), confirming our in vitro findings that IL-17A stimulated the production of proinflammatory cytokines and chemokines in CFs. However, the levels of *Ccl2* and *Lif* were comparable between CFs from WT and *Il17ra*$^{-/-}$ mice (unpublished data), indicating that more complex pathways were involved. Endothelial cells (ECs) have also been reported to respond to IL-17A signals. We therefore also isolated $CD45^-CD34^+CD146^+CD44^{lo}CD31^{hi}$ ECs by FACS from the hearts of WT mice on day 21 of EAM (Fig. 7 A). qPCR analysis showed that the mRNA levels of proinflammatory cytokines and chemokines of interest were dramatically higher in CFs than ECs, with the exception of *Csf3* (Fig. 7 C), indicating that, among cardiac-resident cells, CFs are the dominant source of proinflammatory cytokines and chemokines upon IL-17A stimulation during EAM and DCMi.

CXCL1 is a major chemokine for neutrophil chemotaxis, and the induction of CXCL1 in CFs by IL-17A helps explain the differences in the composition of heart-infiltrating myeloid cells between *Il17ra*$^{-/-}$ and WT mice. Moreover, GM-CSF, G-CSF, and IL-6 play important roles in the differentiation and activation of myeloid cells, suggesting further interactions of CFs and inflammatory cells under IL-17A stimulation.

IL-17A is able to drive the differentiation of monocytes in trans through CFs

To determine whether IL-17A is able to instruct the differentiation of monocytes by inducing cytokine production from CFs, we designed an in vitro fibroblast–monocyte co-culture system. Because spleen is the major reservoir of monocytes during cardiac inflammation (Swirski et al., 2009), $Ly6G^-CD11c^-CD11b^+F4/80^-Ly6C^{hi}$ monocytes were FACS sorted from naive *Il17ra*$^{-/-}$ mouse spleen and co-cultured with primary adult mouse CFs. To exclude direct signaling of IL-17A to monocytes, we used *Il17ra*$^{-/-}$ mice as monocyte donors. *Il17ra*$^{-/-}$ $Ly6C^{hi}$ monocytes were co-cultured with WT CFs for 48 h with or without rIL-17A stimulation. Because monocytes themselves produce TNF, no rTNF was added

viable cells from respective cultures were plotted on histograms. Data are representative of 2 independent experiments. (C) CFs from naive WT mice were cultured with 100 ng/ml rIL-17A, 5 ng/ml rTNF, or two cytokines combined for 24 h. Supernatants were collected after culture, and the levels of CXCL1, CCL2, GM-CSF, G-CSF, IL-6, and LIF were measured by ELISA. (D–F) CFs from naive WT mice were cultured with 100 ng/ml rIL-17A, 5 ng/ml rTNF, or two cytokines combined for 6 h. RNA were isolated from CFs and the mRNA levels of *Cxcl1*, *Ccl2*, *Csf2*, *Csf3*, *Il6*, and *Lif* (D), *Col1a1* and *Col3a1* (E), and *Cx3cl1* (F) were determined by real-time qPCR and normalized to housekeeping gene *Hprt*. (C–F) Data are representative of 3 independent experiments. Data are shown as mean + SEM of 3 replicates and analyzed by one-way ANOVA followed by Tukey's post-test. *, $P < 0.05$; **, $P < 0.01$; ***, $P < 0.001$; ****, $P < 0.0001$; n.s. = not significant.

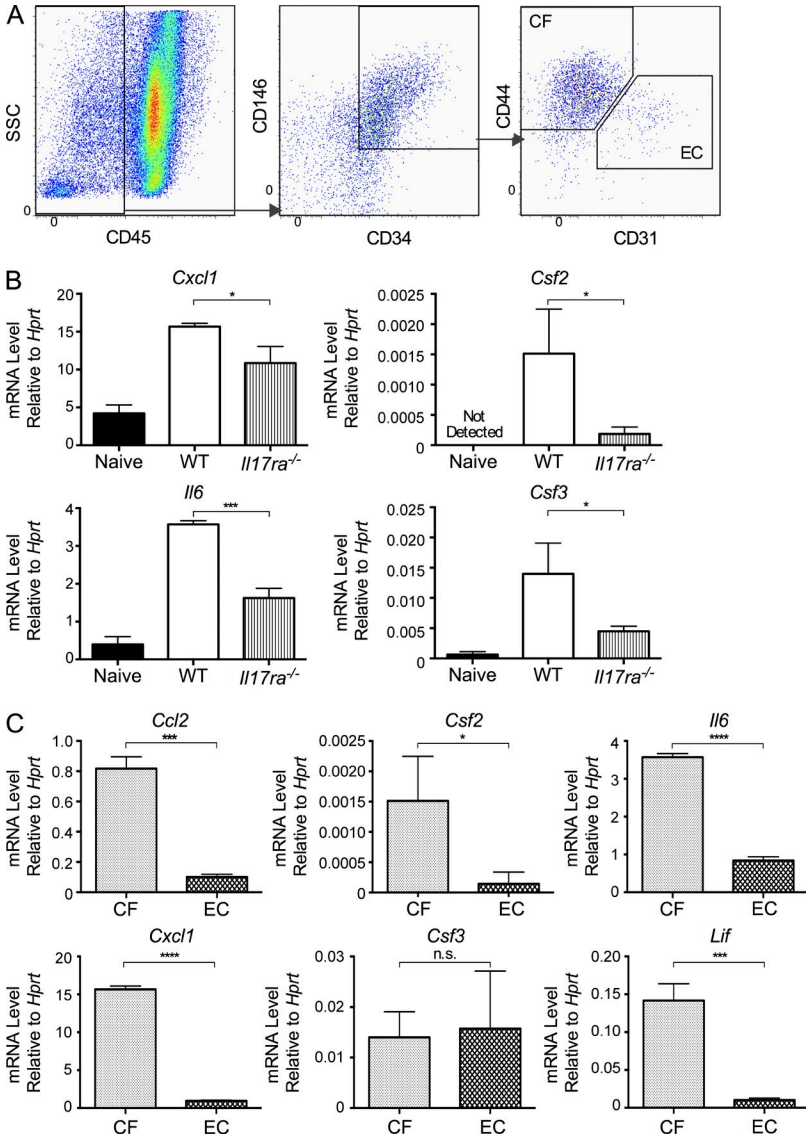

Figure 7. CFs react to IL-17A to produce proinflammatory cytokines and chemokines in vivo. EAM and DCMi were induced in WT and *Il17ra*$^{-/-}$ mice. Mice were sacrificed 21 d after immunization. CD45^{-}CD34^{+}CD146^{+}CD44^{hi}CD31^{-} CFs and CD45^{-}CD34^{+}CD146^{+}CD44^{lo}CD31^{hi} ECs were isolated from mouse hearts by FACS. (A) Representative gating of CFs and ECs from viable singlets. (B) mRNA levels of *Cxcl1*, *Csf2*, *Csf3*, and *Il6* in CFs from WT and *Il17ra*$^{-/-}$ mice were determined by qPCR and normalized to housekeeping gene *Hprt*. (C) mRNA levels of *Ccl2*, *Cxcl1*, *Csf2*, *Csf3*, *Il6*, and *Lif* in CFs and ECs from WT mice were determined by qPCR and normalized to housekeeping gene *Hprt*. For bar graphs, data are representative of 2 independent experiments. Data are shown as mean + SEM of 3 replicates and analyzed by unpaired two-tailed Student's *t* test. *, $P < 0.05$; ***, $P < 0.001$; ****, $P < 0.0001$; n.s. = not significant.

to the cultures. After 48 h of co-culture, monocytes were separated from CFs by FACS. qPCR assay of monocytes showed that, through its effects on CFs, IL-17A was able to indirectly up-regulate proinflammatory genes *Il1b*, *Il6*, *Il12a*, and *Nos2*, while down-regulating suppressive gene *Il10* (Fig. 8 A). We repeated the experiment with *Il17ra*$^{-/-}$ CFs. rIL-17A failed to induce significant difference in *Il17ra*$^{-/-}$ monocytes (Fig. 8 B) without responding CFs, demonstrating that these effects were IL-17A–specific. IL-17A, however, could not induce de novo conversion of Ly6C^{lo} MO/MΦs to Ly6C^{hi} MO/MΦs either directly or indirectly through CFs. rIL-17 failed to affect the Ly6C^{hi} to Ly6C^{lo} ratio in Ly6G^{-}CD11c^{-}CD11b^{+}F4/80^{-} monocytes isolated from the spleen of WT mice (Fig. 8 C). Co-culture of splenic Ly6G^{-}CD11c^{-}CD11b^{+}F4/80^{-} monocytes from *Il17ra*$^{-/-}$ mice with WT CFs resulted in lower level of Ly6C^{hi} MO/MΦs, likely due to phagocytosis-induced conversion (Ramachandran et al., 2012). However, addition of rIL-17A had no additional effects (Fig. 8 D). Thus, IL-17A induced proinflammatory changes in Ly6C^{hi} monocytes indirectly through CFs, suggesting that CFs actively participate in immune response and serve as a mediator between IL-17A and Ly6C^{hi} monocytes.

IL-17A drives the differentiation of monocytes by inducing GM-CSF production in CFs

We have shown that IL-17A induces the production of IL-6, G-CSF, and GM-CSF from CFs (Fig. 6, C and D; and Fig. 7 B), which are all potent drivers of myeloid cells differentiation and activation. We therefore blocked these cytokines with neutralizing antibodies in our CF/monocyte co-culture system to determine which cytokine is the main transducer of the IL-17A signals to monocytes. Anti–IL-6RA mAb and anti–G-CSF mAb both failed to reverse the effect of IL-17A (unpublished data). However, anti–GM-CSF mAb

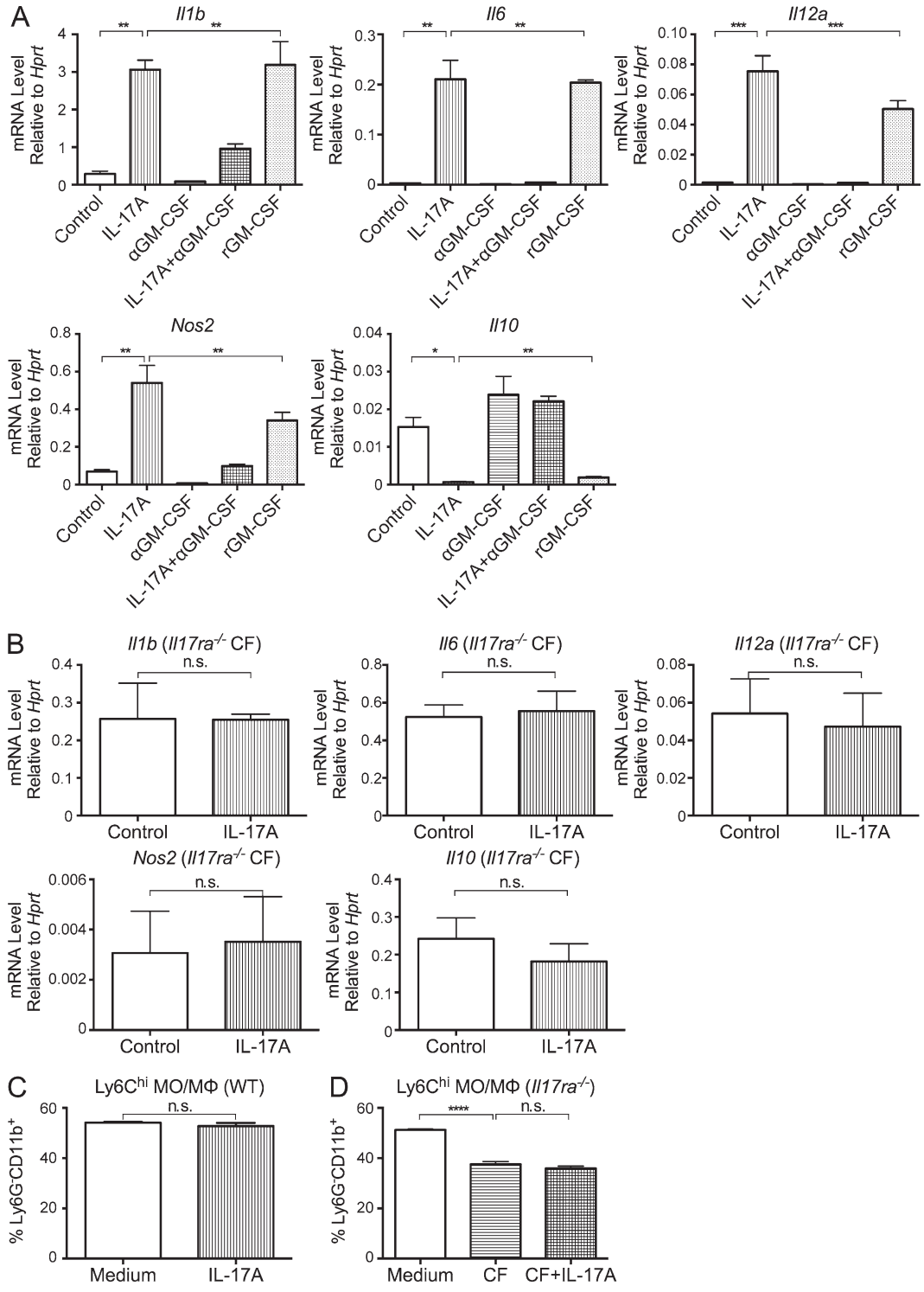

Figure 8. IL-17A drives the differentiation of monocytes in trans through CFs and GM-CSF, but has no effect in the balance of Ly6C^{hi} and Ly6C^{lo} populations. (A) Ly6G$^-$CD11c$^-$CD11b$^+$F4/80$^-$Ly6C^{hi} spleen monocytes were isolated from naive *Il17ra*$^{-/-}$ mice by FACS, and co-cultured with primary adult CFs from naive WT mice for 48 h under various conditions as depicted. mRNAs were isolated from FACS-sorted monocytes in the end of co-culture. The mRNA levels of *Il1b*, *Il6*, *Il12*a, *Nos2*, and *Il10* were measured by real-time qPCR, and normalized to *Hprt*. Data are representative of 3 independent experiments. (B) Ly6G$^-$CD11c$^-$CD11b$^+$F4/80$^-$Ly6C^{hi} spleen monocytes were isolated from naive *Il17ra*$^{-/-}$ mice by FACS, and co-cultured with primary adult CFs from naive *Il17ra*$^{-/-}$ mice for 48 h with or without 100 ng/ml rIL-17A. mRNAs were isolated from FACS-sorted monocytes in the end of co-culture. The mRNA levels of *Il1b*, *Il6*, *Il12*a, *Nos2*, and *Il10* were measured by real-time qPCR and normalized to *Hprt*. (C) Ly6G$^-$CD11c$^-$CD11b$^+$F4/80$^-$ splenic monocytes with mixed Ly6C^{hi} and Ly6C^{lo} populations were isolated from naive WT mice by FACS, and stimulated with 100 ng/ml rIL-17A for 48 h. Ly6C^{hi} monocyte as a proportion of total was analyzed by

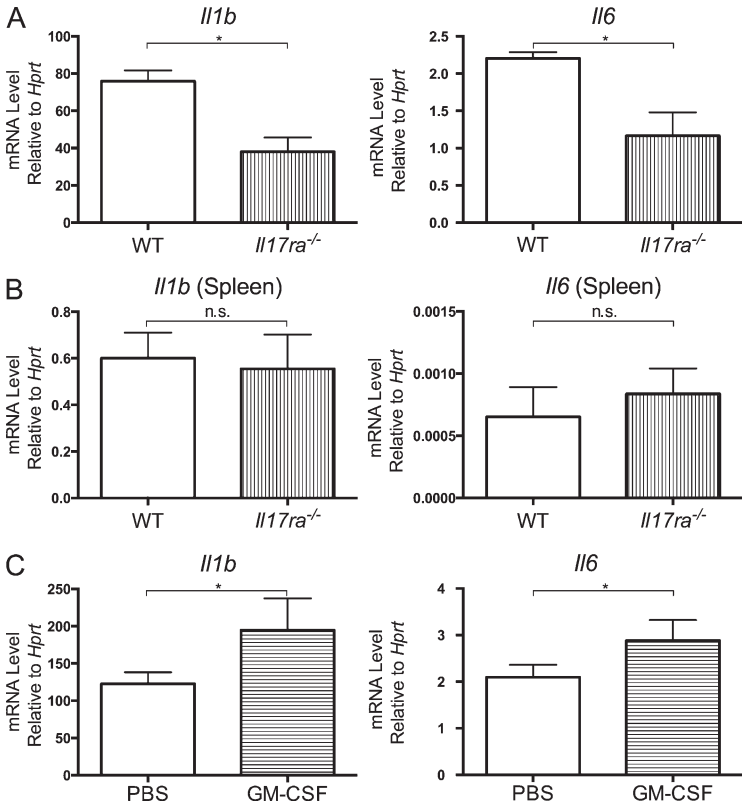

Figure 9. IL-17A and GM-CSF drive cardiac infiltration of Ly6C^{hi} MO/MΦs into proinflammatory phenotype in vivo. (A and B) EAM and DCMi were induced in WT and *Il17ra*$^{-/-}$ mice. Mice were sacrificed 21 d after immunization. (A) Ly6G^{-}CD11b^{+}Ly6C^{hi} MO/MΦs were isolated from mouse hearts by FACS. (B) Ly6G^{-}CD11c^{-}CD11b^{+}F4/80^{-}Ly6C^{hi} monocytes were isolated from mouse spleens by FACS. (C) EAM and DCMi were induced in WT mice. Mice were injected i.p. with PBS or 0.5 µg rGM-CSF, 36 and 12 h before sacrifice at day 21. Ly6G^{-}CD11b^{+}Ly6C^{hi} MO/MΦs were isolated from mouse hearts by FACS. (A–C) mRNA levels of *Il1b* and *Il6* were determined by qPCR and normalized to housekeeping gene *Hprt*. Data are representative of 2 independent experiments. Data are shown as mean + SEM of 3 replicates and analyzed by unpaired two-tailed Student's *t* test. *, P < 0.05; n.s. = not significant.

strongly suppressed the indirect effect of IL-17A on Ly6C^{hi} monocytes (Fig. 8 A). Moreover, the phenotype of monocytes co-cultured with rGM-CSF resembled monocytes from the rIL17A-stimulated co-culture (Fig. 8 A). Therefore, IL-17A induces GM-CSF production from CFs, which mediates the proinflammatory differentiation of Ly6C^{hi} monocytes.

Il17ra$^{-/-}$ mice have less proinflammatory Ly6C^{hi} MO/MΦ infiltration in vivo

We have shown that IL-17A instructs proinflammatory differentiation of Ly6C^{hi} monocytes by inducing GM-CSF production in vitro (Fig. 8 A). To investigate whether IL-17A drives MO/MΦs into a proinflammatory phenotype in the heart, we isolated Ly6C^{hi} MO/MΦs from the hearts of WT or *Il17ra*$^{-/-}$ mice at the peak of inflammation (day 21). Because IL-17A directs proinflammatory changes in monocytes in vitro, we expected that Ly6C^{hi} MO/MΦs from *Il17ra*$^{-/-}$ mice hearts would possess a less inflammatory phenotype due to lack of IL-17RA signaling. qPCR assay showed that Ly6C^{hi} MO/MΦs from *Il17ra*$^{-/-}$ mice hearts produced lower levels of proinflammatory cytokines *Il1b*, *Il6* (Fig. 9 A), mirroring the phenotype observed from in vitro co-culture experiments. Importantly, Ly6C^{hi} monocytes isolated from the spleens of *Il17ra*$^{-/-}$ mice had expression of *Il1b* and *Il6* comparable to WT splenic Ly6C^{hi} monocytes (Fig. 9 B), demonstrating that the effects of IL-17A on MO/MΦs was a local phenomenon specific to the heart during EAM.

To confirm the in vitro results that GM-CSF mediates these effects, we injected immunized WT mice with rGM-CSF, 36 and 12 h before sacrifice on day 21 of EAM, and isolated Ly6C^{hi} MO/MΦs from the hearts by FACS. qPCR analysis showed that Ly6C^{hi} MO/MΦs from the hearts of rGM-CSF–treated mice had higher levels of *Il1b* and *Il6* expression compared with controls injected with PBS (Fig. 9 C), illustrating that GM-CSF elicits proinflammatory polarization of Ly6C^{hi} MO/MΦs MO/MΦs during EAM and DCMi.

Thus, we confirmed our previous in vitro results in vivo, underscoring that IL-17A and GM-CSF directs the polarization of cardiac MO/MΦs and the development of DCMi after EAM. However, Ly6C^{hi} MO/MΦs from *Il17ra*$^{-/-}$ mice expressed comparable levels of *Il12a*, *Nos2*, and *Il10* (unpublished data), which is not consistent with the findings from in vitro co-culture experiment. This difference highlights the complexity of the in vivo inflammatory environment and suggests that other pathways play a role in the programming of MO/MΦs at the site of inflammation.

flow cytometry. (D) Ly6G^{-}CD11c^{-}CD11b^{+}F4/80^{-} splenic monocytes with mixed Ly6C^{hi} and Ly6C^{lo} populations were isolated from naive *Il17ra*$^{-/-}$ mice by FACS, and cultured alone (medium), with WT CFs (CF), or with WT CF and rIL-17A (CF+IL-17A) for 48 h. Ly6C^{hi} monocyte as a proportion of total was analyzed by flow cytometry. (B–D) Data are representative of 2 independent experiments. (A–D) Data are shown as mean + SEM of 3 replicates and analyzed by and one-way ANOVA followed by Tukey's post-test (A and D), or unpaired two-tailed Student's *t* test (B and C). *, P < 0.05; **, P < 0.01; ***, P < 0.001; ****, P < 0.0001; n.s. = not significant.

DISCUSSION

About 9–16% of patients with myocarditis progress to dilated cardiomyopathy (Herskowitz et al., 1993; Sagar et al., 2012), but there are no reliable biological markers that would help identify myocarditis patients with high risk of progressing to DCMi (Cooper, 2009). Currently, a definitive diagnosis of myocarditis depends on a biopsy of the myocardium. Based on the Dallas criteria, the heart is evaluated based on the presence and density of inflammatory infiltration and CM death (Aretz et al., 1987). However, our study clearly shows that not only the quantity but also the quality of these infiltrating cells is critical in predicting the development of DCMi. Similar to *Il17a*$^{-/-}$ mice, *Il17ra*$^{-/-}$ mice developed myocarditis and had overall CD45^{+} cell infiltration comparable to WT, but were nonetheless not susceptible to DCMi. This protection is associated with a different infiltration profile. *Il17ra*$^{-/-}$ mice had diminished infiltration of neutrophils, which have been implicated in inducing cardiac damage and rupture in a myocardial infarction model (Vinten-Johansen, 2004; Hiroi et al., 2013). A recent study revealed that neutrophils also play an important role in the recruitment of monocytes (Wantha et al., 2013). In addition, *Il17ra*$^{-/-}$ mice had significantly less infiltration of proinflammatory monocytes and lower Ly6C^{hi} to Ly6C^{lo} MO/MΦ ratios specifically in their heart, which represents a potentially useful biomarker for DCMi risk in myocarditis patients.

Monocytes and macrophages are key effector cells in EAM (Barin et al., 2012) as well as in human giant cell myocarditis (Cooper et al., 2007). MO/MΦs are not a homogeneous population (Hashimoto et al., 2011). However, cardiac disease literature tended to ignore their heterogeneity until recently, leading to substantial disagreement in reported findings. During early development, progenitor cells migrate into solid organs and develop into tissue-resident macrophages, which are maintained by local proliferation with minimal replenishment from blood monocytes (Hashimoto et al., 2013; Yona et al., 2013). During an inflammatory process, blood monocytes rapidly migrate to the site of inflammation, where they mature into macrophages in response to local stimulating signals (Sica and Mantovani, 2012). In mouse, monocytes form two major subsets in blood, CCR2^{hi}CX3CR1^{lo}Ly6C^{hi} (resembling human CD14^{hi}CD16^{-} monocytes) and CCR2^{lo} CX3CR1^{hi}Ly6C^{lo} (resembling human CD14^{lo}CD16^{+} monocytes; Geissmann et al., 2003; Shi and Pamer, 2011).

In our study, the balance of these two MO/MΦs subsets in the heart determines the outcome of inflammation. Thus, IL-17RA deficiency leads to a lower Ly6C^{hi}/Ly6C^{lo} ratio and protection from DCMi. We found that heart-infiltrating Ly6C^{hi} MO/MΦs had a proinflammatory and profibrotic phenotype. The proinflammatory cytokines and TGF-β activators they produce are likely to play critical roles in cardiac remodeling. Ly6C^{lo} monocytes in heart produced high levels of MMPs and IGF-1, which have been described as protective in fibrosis (Ramachandran et al., 2012; Bessich et al., 2013). We used two methods to manipulate the balance of Ly6C^{hi} and Ly6C^{lo} MO/MΦs to demonstrate the role they play in DCMi: First, depletion of Ly6G^{-}CD11b^{+} MO/MΦs by clodronate-loaded liposomes also lowered the ratio of Ly6C^{hi} to Ly6C^{lo} MO/MΦs in the heart. Second, PBS-loaded liposomes specifically lowered the ratio of Ly6C^{hi} to Ly6C^{lo} MO/MΦs without affecting the total number of MO/MΦs in the heart. Neither method induced any change in severity of myocarditis, but both protected mice from cardiac fibrosis and the development of severe DCMi, demonstrating that Ly6C^{hi} MO/MΦs aggravate the development of DCMi. Similarly, in a heart ischemia/reperfusion model, early recruitment of Ly6C^{hi} monocytes is associated with injury, preceding the recruitment of Ly6C^{lo} monocytes, which appear to be involved in myocardial healing (Nahrendorf et al., 2007). Ly6C^{lo} monocytes were shown to be able to arrest and reverse fibrosis in a model of CCl_4-induced liver damage (Ramachandran et al., 2012).

We further suggest that the M1/M2 paradigm does not perfectly overlap with Ly6C^{hi} and Ly6C^{low} subsets and does not accurately describe these two different populations in the heart during EAM. Traditionally, M1 represents a population that promotes inflammation, whereas M2 is responsible for tissue repair and fibrosis (Gordon and Taylor, 2005). However, in our EAM model, Ly6C^{hi} MO/MΦs have a proinflammatory and profibrotic phenotype. They up-regulate classic M1 markers like *Tnf* and *Nos2*, as well as M2 markers like *Chi3l3*, while Ly6C^{lo} MO/MΦs produced molecules that are believed to help resolve fibrosis (Ramachandran et al., 2012; Bessich et al., 2013). Unlike classic tissue-resident macrophage populations in the liver and lung, both Ly6C^{hi} and Ly6C^{lo} MO/MΦs in the heart express very dim levels of classic murine macrophage marker F4/80, and the levels are comparable between Ly6C^{hi} and Ly6C^{lo} populations; in contrast, Ly6C^{lo} population expresses CD11c and MHC II at higher levels than Ly6C^{hi} MO/MΦs (unpublished data). However, we did not observe the discrepancy in MHC II expression within Ly6C^{lo} population recently described by Epelman et al. (2014); in our EAM model, all the Ly6C^{lo} MO/MΦs in the heart express high levels of MHC II (not depicted). Recent studies showed more complex relationships between cardiac Ly6C^{hi} and Ly6C^{lo} MO/MΦs, and suggested the conversion between the two in the heart: Hilgendorf et al. (2014) discovered that instead of being recruited from the blood Ly6C^{lo} pool, Ly6C^{lo} MO/MΦs derived from Ly6C^{hi} MO/MΦs in the heart; Epelman et al. (2014) demonstrated that the Ly6C^{lo} population arises during early development, and is maintained through distinct mechanisms at steady state and during inflammation. In our EAM model, using a BrdU pulse approach, we also found that cardiac Ly6C^{hi} MO/MΦs undergo rapid turnover, whereas Ly6C^{lo} population was more stable (unpublished data), confirming these findings.

We have shown previously that MO/MΦs express receptors for IL-17A but direct stimulation of MO/MΦs with IL-17A does not induce a proinflammatory phenotype (Barin et al., 2012). BM chimeras revealed that deficiency of IL-17A/IL-17RA signaling in nonhematopoietic cells is sufficient to suppress the augmentation of immune response and protect mice

from cardiac damage. In addition, IL-17A signaling to cardiac-resident cells was essential for the IL-17A–driven recruitment of neutrophils and Ly6C^{hi} monocytes to the inflamed heart.

A recent study found that IL-17A was able to induce apoptosis in neonatal CMs in vitro (Liao et al., 2012). The authors suggested that this effect contributed to CM death during myocardial infarction in adult mice. Other investigators reported that IL-17A induced collagen production in neonatal CFs (Liu et al., 2012). However, neonatal cells have unique properties that are not retained in adult cells and are not necessarily the appropriate model to study adult diseases. We observed that IL-17A neither induced apoptosis nor activated the NF-κB pathway in primary adult CMs in vitro, indicating that CMs are not likely to be the primary target of IL-17A in adults. In addition, IL-17A did not directly stimulate collagen production in adult CFs.

In contrast, adult CFs respond to IL-17A by producing high levels of chemokines and cytokines known to facilitate myeloid cell recruitment and instruct their in situ differentiation toward an inflammatory phenotype. CFs isolated from *Il17ra*$^{-/-}$ mice during EAM expressed significantly lower levels of proinflammatory cytokines and chemokines. Importantly, although it was reported that ECs react to IL-17A stimulation, they produced a minimal amount of cytokines and chemokines compared with CFs; hence, ECs do not appear to be the primary target of IL-17A in our model of EAM and DCMi. Thus, our study highlights the central, decisive role that non-immune cells like fibroblasts can play in immunological processes. CFs served as a critical mediator between adaptive and innate immune cells and actively participated in the augmentation of immune response. In response to IL-17A stimulation from adaptive T cells, CFs produce granulocytic and monocytic chemokines to recruit innate effector cells and aggravate the immune response. CFs also secrete cytokines, in this case GM-CSF, to direct these recruited MO/MΦ effectors to a more proinflammatory phenotype, which further intensifies inflammation. Moreover, this mediator role played by CFs proved crucial in DCMi, as deficiency of IL-17A/IL-17RA signaling in nonhematopoietic cells was sufficient to protect mice from cardiac damage.

Our studies also revealed that the main mediator of local communications between CFs and MO/MΦs was CF-derived GM-CSF. GM-CSF is known to elicit the expansion and differentiation of progenitors of the myeloid lineages; GM-CSF also supports the survival and activation of effector functions of myeloid cells (Papatriantafyllou, 2011). In ischemic heart disease, although associated with poor prognosis (Maekawa et al., 2004), GM-CSF has been studied largely for its role outside of its immunological functions. These mechanisms mostly involve angiogenesis or the mobilization of hematopoietic stem cell–like cells (Zbinden et al., 2005). There have also been attempts to study the role of GM-CSF in myocarditis: Blyszczuk et al. (2013) argued that GM-CSF does not affect dendritic cell functions during the effector phase of EAM; however, they neglected to address the effects of GM-CSF on MO/MΦs and their impact on cardiac damage. Our data now point to GM-CSF acting as a key mediator of IL-17A–driven autoimmunity in DCMi: IL-17A signaling induces GM-CSF production from CFs. GM-CSF then drives differentiation of heart-infiltrating MO/MΦs toward a proinflammatory phenotype that in turn promotes DCMi.

In conclusion, our study demonstrates that the IL-17A–IL-17RA axis is critical in the development of DCMi, a fatal inflammatory heart disease. IL-17A induces chemokine production by CFs, resulting in an infiltrate rich in neutrophils and Ly6C^{hi} MO/MΦs in the heart. Furthermore, IL-17A directs monocytic infiltrates into an even more inflammatory phenotype by inducing GM-CSF production from CFs. This novel pathway provides new potential markers to identify myocarditis patients with a high risk of developing DCMI. This pathway further suggests new targets for the prevention of DCMi. In addition, other groups have shown that IL-17A is critical in inflammatory diseases including myocardial ischemia/reperfusion injury (Liao et al., 2012), pulmonary fibrosis (Wilson et al., 2010), and liver cirrhosis (Kono et al., 2011). The pathway involving IL-17A, fibroblasts, GM-CSF, and MO/MΦs may therefore play a key role in many other diseases.

MATERIALS AND METHODS

Mice. *Il17ra*$^{-/-}$ founder mice backcrossed eight generations from C57BL/6 to BALB/c background were provided by Amgen Inc. and J. Kolls (Children's Hospital of Pittsburgh of University of Pittsburgh Medical Center, Pittsburgh, PA; Yu et al., 2008). WT BALB/cJ and CBy.PL(B6)-Thy1a/ScrJ (Thy1.1) founder mice were purchased from The Jackson Laboratory. *Il17ra*$^{-/-}$ mice were crossed to Thy1.1 mice and bred to homozygosity at both loci for the generation of BM chimeras. All mice were maintained in the Johns Hopkins University School of Medicine specific pathogen-free vivarium. Age-matched WT, Thy1.1, and *Il17ra*$^{-/-}$ mice bred separately in the Johns Hopkins vivarium were used for experiments involving multiple gene backgrounds. For experiments conducted exclusively on WT background, WT BALB/cJ (000651) mice (The Jackson Laboratory) were housed in the Johns Hopkins vivarium for a week before immunization. Experiments were conducted on 6–10-wk-old male mice, and in compliance with the Animal Welfare Act and the principles set forth in the Guide for the Care and Use of Laboratory Animals. All methods and protocols are approved by the Animal Care and Use Committee of The Johns Hopkins University.

Induction of EAM and DCMi. We used the myocarditogenic peptide MyHCα$_{614-629}$ (Ac-SLKLMATLFSTYASAD) commercially synthesized by fMOC chemistry and purified to a minimum of 90% by HPLC (Genscript). On days 0 and 7, mice received axillary s.c. immunizations of 100 µg MyHCα$_{614-629}$ peptide emulsified in CFA (Sigma-Aldrich) supplemented to 5 mg/ml of heat-killed *M. tb* strain H37Ra (Difco). On day 0, mice also received 500 ng pertussis toxin i.p. (List Biologicals).

Assessment of EAM and DCMi histopathology. Mice were evaluated for the development of EAM and DCMi on days 21 and 63, respectively. Heart tissues were fixed in SafeFix solution (Thermo Fisher Scientific). Tissues were embedded longitudinally, and 5-µm serial sections were cut and stained with H&E or Masson's trichrome blue (HistoServ). Myocarditis severity was evaluated by H&E staining of myocardium area infiltrated with hematopoietic cells, according to the following scoring system: grade 0, no inflammation; grade 1, <10% of the heart section is involved; grade 2, 10–25%; grade 3, 25–50%; grade 4, 50–75%; grade 5, >75%. Grading was performed by grading five sections per heart by two independent, blinded investigators and averaged. Cardiac fibrosis was evaluated by measuring the area of blue staining of fibrosis as a proportion of heart cross section.

Echocardiography. Trans-thoracic echocardiography was performed using the Acuson Sequoia C256 ultrasonic imaging system (Siemens). Conscious, depilated mice were held in supine position. The heart was imaged in two-dimensional (2-D) mode in the parasternal short axis view. From this mode, an M-mode cursor was positioned perpendicular to the interventricular septum (IVS) and the left ventricular posterior wall (LVPW) at the level of the papillary muscles. From M-mode, the wall thicknesses and chamber dimensions were measured. For each mouse, three to five values for each measurement were obtained and averaged for evaluation. The left ventricular end-diastolic dimension (LVEdD), LV end-systolic dimension (LVEsD), interventricular septal wall thickness at end-diastole (IVSD), and LV posterior wall thickness at end diastole (LVPWTED) were measured from a frozen M-mode tracing. Fractional shortening (FS), ejection fraction (EF), and relative wall thickness (RWT) were calculated from these parameters as previously described (Baldeviano et al., 2010).

Hydroxyproline assay. Heart samples were weighed, homogenized in de-ionized water, and then hydrolyzed in 6N HCl overnight at 120°C. Lysates are transferred and desiccated in 96-well plates, and reconstituted in de-ionized water. After incubation with 50 mM Chloramine T (Sigma-Aldrich), followed by 1 M dimethylaminobenzaldehyde (Sigma-Aldrich), the OD values were read at 570 nm. The concentration of hydroxyproline was determined by a 1–100 µg/ml standard curve of hydroxyproline (Sigma-Aldrich) and normalized to starting heart sample mass.

Flow cytometry analysis and FACS isolation of heart infiltrating cells, CFs, and ECs. For flow cytometry analysis, single cell suspensions were made from mouse spleen by gentle dissociation or from mouse hearts by perfusing for 3 min with 1× PBS + 0.5% FBS, and digested in gentleMACS C Tubes according to manufacturer's instructions (Miltenyi Biotec). Viability was determined by LIVE/DEAD staining according to manufacturer's instructions (Life Technologies). Cells were blocked with α-CD16/32 (eBioscience), and surface markers were stained with fluorochrome-conjugated mAbs (eBioscience, BD, and BioLegend). Samples were acquired on the LSR II cytometer running FACSDiva 6 (BD). Data were analyzed with FlowJo 7.6 (Tree Star). For FACS isolation, single cell suspension from mouse heart or spleen was first purified with a 20–80% Percoll (GE Healthcare) gradient to eliminate dead cells and debris. Cells were then stained with fluorochrome-conjugated mAbs (eBioscience, BD, and BioLegend) and sorted with a MoFlo Cell Sorter (Beckman Coulter).

Treatment of PBS-loaded or clodronate-loaded liposomes and rGM-CSF during EAM and DCMi. PBS-loaded and clodronate-loaded liposomes were purchased from ClodLip BV (Haalem). Recombinant mouse GM-CSF was purchased from R&D Systems. For liposome treatment, 250 µl PBS, PBS-loaded, or clodronate-loaded liposomes were injected intravenously via the tail vein every other day. For rGM-CSF treatment, PBS or 0.5 µg rGM-CSF in 200 µl PBS were injected i.p.

qPCR. Tissue total RNA was extracted in TRIZOL (Life Technologies). cDNAs were synthesized with the High Capacity cDNA Reverse Transcription kit (Life Technologies) and amplified with Power SYBR Green master mix (Life Technologies) in MyiQ2 thermocycler (Bio-Rad Laboratories) running iQ5 software (Bio-Rad Laboratories). Data were analyzed by the $2-\Delta\Delta$Ct method of (Livak and Schmittgen, 2001), comparing threshold cycles first to *Hprt* expression, and then ΔCt of target genes in controls.

Generation of BM chimera mice. Thy1.2$^+$ WT or *Il17ra*$^{-/-}$ recipient mice were irradiated with two doses of 600 rad irradiation within 4 h. 24 h later, they were reconstituted with 10×10^6 Thy1.1$^+$ WT or *Il17ra*$^{-/-}$ donor BM cells i.v. Animals were allowed to reconstitute for a minimum of 8 wk before EAM induction.

Isolation of primary adult mouse CMs and CFs. Hearts were dissected from 6–8-wk-old male mice pretreated with heparin, aorta were cannulated, and hearts were perfused with calcium-free perfusion buffer, and digested by type II collagenase (Worthington Biochemical Corporation). CMs were separated from resulting suspensions by their rapid spontaneous precipitation. Isolated CMs were cultured in mouse laminin-coated plates or chamber slides and used for experiments after 24 h. CFs and other cell populations remain in supernatant and were seeded on uncoated plates in DMEM with 4.5 g/liter glucose, 2 mM L-glutamine, 1 mM sodium pyruvate, 25 mM Hepes, 100 U/ml penicillin G, 100 µg/ml streptomycin, 250 ng/ml amphotericin B, and 20% FBS. Nonadherent cells were washed off after 45 min. Infiltrating hematopoietic cells die off in high FBS media due to cytokine exhaustion, resulting in CF culture.

Western blot. Cells were collected in RIPA buffer (Sigma-Aldrich), and total protein was quantified by BCA assay (Thermo Fisher Scientific). 20 µg of sample were separated with 10% SDS-PAGE with Mini-Protean precast gels (Bio-Rad Laboratories). After transfer to PVDF membrane (Bio-Rad Laboratories), IκBα was blotted with mAb clone L35A5 (Cell Signaling Technology), and β-actin was blotted with mAb clone 13E5 (Cell Signaling Technology). HRP-conjugated secondary antibodies (Jackson ImmunoResearch Laboratories, Inc.) and Amersham ECL Prime detection system (GE Healthcare) was used to visualize the bands.

BM-derived macrophage. BM cells from femur and tibia were isolated from adult WT BALB/cJ mice and cultured in DMEM with 4.5 g/liter glucose, 2 mM L-glutamine, 1 mM sodium pyruvate, 25 mM Hepes, 100 U/ml penicillin G, 100 µg/ml streptomycin, 55 µM 2-mercaptoethanol, and 10% FBS supplemented with 10 ng/ml recombinant M-CSF (R&D Systems) for 8 d.

Immunofluorescence microscopy. CFs and BM-derived macrophages were grown on chamber slides (Thermo Fisher Scientific). Cells were fixed with 4% paraformaldehyde and permeabilized with 0.1% Triton X-100 (Sigma-Aldrich). After blocking with donkey serum, cells were incubated with anti–α-SMA (Abcam) and anti–mouse CD11b (eBioscience clone M1/70) antibodies. FITC-conjugated donkey anti–rabbit and Texas red–conjugated donkey anti–rat secondary antibodies with minimal cross reactivity (Jackson ImmunoResearch Laboratories) were then used. Cells were counterstained by DAPI. Images were acquired by an Eclipse 90i microscope (Nikon) at 20× magnification and Volocity image analysis software (PerkinElmer).

ELISA. Quantitative sandwich ELISA for cell culture supernatants were determined by colorimetric ELISA kits according to the manufacturers' recommended protocols (R&D Systems).

Statistics. Normally distributed data were analyzed by two-tailed Student's *t* test (up to two groups), one-way ANOVA followed by Tukey's post-test, or two-way ANOVA (multiple factor analysis) followed by Tukey's post-test. EAM severity scores were analyzed by Mann-Whitney *U* test. Values of $P < 0.05$ were considered statistically significant.

The authors would like to extend their gratitude to Amgen Inc. and Dr. Jay Kolls for providing *Il17ra*$^{-/-}$ mice, to Dr. Fengyi Wan and Teng Han for assistance with Western blotting, to Dr. Norimichi Koitabashi for assistance with the isolation of CMs and CFs, to Dr. Alessandra de Remigis for assistance with immunofluorescence microscopy, and to Xiaoling Zhang and Tricia Nilles for assistance with flow cytometry.

L. Wu is the O'Leary-Wilson Fellow in Autoimmune Disease Research in Johns Hopkins Autoimmune Disease Research Center. S. Ong is the recipient of the Ruth L. Kirschstein National Research Service Award from National Institutes of Health (NIH). D. Čiháková was supported by the Michel Mirowski MD Discovery Foundation, the W.W. Smith Charitable Trust heart research grant H1103, and The Children's Cardiomyopathy Foundation. This work was further supported by NIH/NHLBI grants R01HL118183 (D. Čiháková) and R01HL113008 (N.R. Rose).

The authors declare no competing financial interests.

Submitted: 8 October 2013
Accepted: 12 May 2014

REFERENCES

Aretz, H.T., M.E. Billingham, W.D. Edwards, S.M. Factor, J.T. Fallon, J.J. Fenoglio Jr., E.G. Olsen, and F.J. Schoen. 1987. Myocarditis. A histopathologic definition and classification. *Am. J. Cardiovasc. Pathol.* 1:3–14.

Baldeviano, G.C., J.G. Barin, M.V. Talor, S. Srinivasan, D. Bedja, D. Zheng, K. Gabrielson, Y. Iwakura, N.R. Rose, and D. Cihakova. 2010. Interleukin-17A is dispensable for myocarditis but essential for the progression to dilated cardiomyopathy. *Circ. Res.* 106:1646–1655. http://dx.doi.org/10.1161/CIRCRESAHA.109.213157

Barin, J.G., N.R. Rose, and D. Cihákova. 2012. Macrophage diversity in cardiac inflammation: a review. *Immunobiology*. 217:468–475. http://dx.doi.org/10.1016/j.imbio.2011.06.009

Bessich, J.L., A.B. Nymon, L.A. Moulton, D. Dorman, and A. Ashare. 2013. Low levels of insulin-like growth factor-1 contribute to alveolar macrophage dysfunction in cystic fibrosis. *J. Immunol.* 191:378–385. http://dx.doi.org/10.4049/jimmunol.1300221

Blyszczuk, P., S. Behnke, T.F. Lüscher, U. Eriksson, and G. Kania. 2013. GM-CSF promotes inflammatory dendritic cell formation but does not contribute to disease progression in experimental autoimmune myocarditis. *Biochim. Biophys. Acta.* 1833:934–944. http://dx.doi.org/10.1016/j.bbamcr.2012.10.008

Čiháková, D., and N.R. Rose. 2008. Pathogenesis of myocarditis and dilated cardiomyopathy. *Adv. Immunol.* 99:95–114. http://dx.doi.org/10.1016/S0065-2776(08)00604-4

Čiháková, D., R.B. Sharma, D. Fairweather, M. Afanasyeva, and N.R. Rose. 2004. Animal models for autoimmune myocarditis and autoimmune thyroiditis. *Methods Mol. Med.* 102:175–193.

Čiháková, D., J.G. Barin, M. Afanasyeva, M. Kimura, D. Fairweather, M. Berg, M.V. Talor, G.C. Baldeviano, S. Frisancho, K. Gabrielson, et al. 2008. Interleukin-13 protects against experimental autoimmune myocarditis by regulating macrophage differentiation. *Am. J. Pathol.* 172:1195–1208. http://dx.doi.org/10.2353/ajpath.2008.070207

Cooper, L.T. Jr. 2009. Myocarditis. *N. Engl. J. Med.* 360:1526–1538. http://dx.doi.org/10.1056/NEJMra0800028

Cooper, L.T., K.L. Baughman, A.M. Feldman, A. Frustaci, M. Jessup, U. Kuhl, G.N. Levine, J. Narula, R.C. Starling, J. Towbin, and R. Virmani. 2007. The role of endomyocardial biopsy in the management of cardiovascular disease: a scientific statement from the American Heart Association, the American College of Cardiology, and the European Society of Cardiology Endorsed by the Heart Failure Society of America and the Heart Failure Association of the European Society of Cardiology. *Eur. Heart J.* 28:3076–3093. http://dx.doi.org/10.1093/eurheartj/ehm456

Dimas, V.V., S.W. Denfield, R.A. Friedman, B.C. Cannon, J.J. Kim, E.O. Smith, S.K. Clunie, J.F. Price, J.A. Towbin, W.J. Dreyer, and N.J. Kertesz. 2009. Frequency of cardiac death in children with idiopathic dilated cardiomyopathy. *Am. J. Cardiol.* 104:1574–1577. http://dx.doi.org/10.1016/j.amjcard.2009.07.034

Ding, L., H. Hanawa, Y. Ota, G. Hasegawa, K. Hao, F. Asami, R. Watanabe, T. Yoshida, K. Toba, K. Yoshida, et al. 2010. Lipocalin-2/neutrophil gelatinase-B associated lipocalin is strongly induced in hearts of rats with autoimmune myocarditis and in human myocarditis. *Circ. J.* 74:523–530. http://dx.doi.org/10.1253/circj.CJ-09-0485

Epelman, S., K.J. Lavine, A.E. Beaudin, D.K. Sojka, J.A. Carrero, B. Calderon, T. Brija, E.L. Gautier, S. Ivanov, A.T. Satpathy, et al. 2014. Embryonic and adult-derived resident cardiac macrophages are maintained through distinct mechanisms at steady state and during inflammation. *Immunity*. 40:91–104. http://dx.doi.org/10.1016/j.immuni.2013.11.019

Frangogiannis, N.G. 2012. Matricellular proteins in cardiac adaptation and disease. *Physiol. Rev.* 92:635–688. http://dx.doi.org/10.1152/physrev.00008.2011

Gaffen, S.L. 2009. Structure and signalling in the IL-17 receptor family. *Nat. Rev. Immunol.* 9:556–567. http://dx.doi.org/10.1038/nri2586

Geissmann, F., S. Jung, and D.R. Littman. 2003. Blood monocytes consist of two principal subsets with distinct migratory properties. *Immunity*. 19:71–82. http://dx.doi.org/10.1016/S1074-7613(03)00174-2

Gordon, S., and P.R. Taylor. 2005. Monocyte and macrophage heterogeneity. *Nat. Rev. Immunol.* 5:953–964. http://dx.doi.org/10.1038/nri1733

Hashimoto, D., J. Miller, and M. Merad. 2011. Dendritic cell and macrophage heterogeneity in vivo. *Immunity*. 35:323–335. http://dx.doi.org/10.1016/j.immuni.2011.09.007

Hashimoto, D., A. Chow, C. Noizat, P. Teo, M.B. Beasley, M. Leboeuf, C.D. Becker, P. See, J. Price, D. Lucas, et al. 2013. Tissue-resident macrophages self-maintain locally throughout adult life with minimal contribution from circulating monocytes. *Immunity*. 38:792–804. http://dx.doi.org/10.1016/j.immuni.2013.04.004

Herskowitz, A., S. Campbell, J. Deckers, E.K. Kasper, J. Boehmer, D. Hadian, D.A. Neumann, and K.L. Baughman. 1993. Demographic features and prevalence of idiopathic myocarditis in patients undergoing endomyocardial biopsy. *Am. J. Cardiol.* 71:982–986. http://dx.doi.org/10.1016/0002-9149(93)90918-3

Hilgendorf, I., L.M. Gerhardt, T.C. Tan, C. Winter, T.A. Holderried, B.G. Chousterman, Y. Iwamoto, R. Liao, A. Zirlik, M. Scherer-Crosbie, et al. 2014. Ly-6C^{high} monocytes depend on Nr4a1 to balance both inflammatory and reparative phases in the infarcted myocardium. *Circ. Res.* 114:1611–1622. http://dx.doi.org/10.1161/CIRCRESAHA.114.303204

Hiroi, T., T. Wajima, T. Negoro, M. Ishii, Y. Nakano, Y. Kiuchi, Y. Mori, and S. Shimizu. 2013. Neutrophil TRPM2 channels are implicated in the exacerbation of myocardial ischaemia/reperfusion injury. *Cardiovasc. Res.* 97:271–281. http://dx.doi.org/10.1093/cvr/cvs332

Kono, H., H. Fujii, M. Ogiku, N. Hosomura, H. Amemiya, M. Tsuchiya, and M. Hara. 2011. Role of IL-17A in neutrophil recruitment and hepatic injury after warm ischemia-reperfusion mice. *J. Immunol.* 187:4818–4825. http://dx.doi.org/10.4049/jimmunol.1100490

Korn, T., E. Bettelli, M. Oukka, and V.K. Kuchroo. 2009. IL-17 and Th17 cells. *Annu. Rev. Immunol.* 27:485–517. http://dx.doi.org/10.1146/annurev.immunol.021908.132710

Lan, R.Y.Z., T.L. Salunga, K. Tsuneyama, Z.-X. Lian, G.-X. Yang, W. Hsu, Y. Moritoki, A.A. Ansari, C. Kemper, J. Price, et al. 2009. Hepatic IL-17 responses in human and murine primary biliary cirrhosis. *J. Autoimmun.* 32:43–51. http://dx.doi.org/10.1016/j.jaut.2008.11.001

Liao, Y.-H., N. Xia, S.-F. Zhou, T.-T. Tang, X.-X. Yan, B.-J. Lv, S.-F. Nie, J. Wang, Y. Iwakura, H. Xiao, et al. 2012. Interleukin-17A contributes to myocardial ischemia/reperfusion injury by regulating cardiomyocyte apoptosis and neutrophil infiltration. *J. Am. Coll. Cardiol.* 59:420–429. http://dx.doi.org/10.1016/j.jacc.2011.10.863

Liu, Y., H. Zhu, Z. Su, C. Sun, J. Yin, H. Yuan, S. Sandoghchian, Z. Jiao, S. Wang, and H. Xu. 2012. IL-17 contributes to cardiac fibrosis following experimental autoimmune myocarditis by a PKCβ/Erk1/2/NF-κB-dependent signaling pathway. *Int. Immunol.* 24:605–612. http://dx.doi.org/10.1093/intimm/dxs056

Livak, K.J., and T.D. Schmittgen. 2001. Analysis of relative gene expression data using real-time quantitative PCR and the $2^{-\Delta\Delta CT}$ Method. *Methods.* 25:402–408. http://dx.doi.org/10.1006/meth.2001.1262

Maekawa, Y., T. Anzai, T. Yoshikawa, Y. Sugano, K. Mahara, T. Kohno, T. Takahashi, and S. Ogawa. 2004. Effect of granulocyte-macrophage colony-stimulating factor inducer on left ventricular remodeling after acute myocardial infarction. *J. Am. Coll. Cardiol.* 44:1510–1520. http://dx.doi.org/10.1016/j.jacc.2004.05.083

Nahrendorf, M., F.K. Swirski, E. Aikawa, L. Stangenberg, T. Wurdinger, J.-L. Figueiredo, P. Libby, R. Weissleder, and M.J. Pittet. 2007. The healing myocardium sequentially mobilizes two monocyte subsets with divergent and complementary functions. *J. Exp. Med.* 204:3037–3047. http://dx.doi.org/10.1084/jem.20070885

Papatriantafyllou, M. 2011. Cytokines: GM-CSF in focus. *Nat. Rev. Immunol.* 11:370–371. http://dx.doi.org/10.1038/nri2996

Pietra, B.A., P.F. Kantor, H.L. Bartlett, C. Chin, C.E. Canter, R.L. Larsen, R.E. Edens, S.D. Colan, J.A. Towbin, S.E. Lipshultz, et al. 2012. Early predictors of survival to and after heart transplantation in children with dilated cardiomyopathy. *Circulation.* 126:1079–1086. http://dx.doi.org/10.1161/CIRCULATIONAHA.110.011999

Ramachandran, P., A. Pellicoro, M.A. Vernon, L. Boulter, R.L. Aucott, A. Ali, S.N. Hartland, V.K. Snowdon, A. Cappon, T.T. Gordon-Walker, et al. 2012. Differential Ly-6C expression identifies the recruited macrophage phenotype, which orchestrates the regression of murine liver fibrosis. *Proc. Natl. Acad. Sci. USA.* 109:E3186–E3195. http://dx.doi.org/10.1073/pnas.1119964109

Ruddy, M.J., G.C. Wong, X.K. Liu, H. Yamamoto, S. Kasayama, K.L. Kirkwood, and S.L. Gaffen. 2004. Functional cooperation between interleukin-17 and tumor necrosis factor-alpha is mediated by CCAAT/enhancer-binding protein family members. *J. Biol. Chem.* 279:2559–2567. http://dx.doi.org/10.1074/jbc.M308809200

Sagar, S., P.P. Liu, and L.T. Cooper Jr. 2012. Myocarditis. *Lancet.* 379:738–747. http://dx.doi.org/10.1016/S0140-6736(11)60648-X

Shi, C., and E.G. Pamer. 2011. Monocyte recruitment during infection and inflammation. *Nat. Rev. Immunol.* 11:762–774. http://dx.doi.org/10.1038/nri3070

Sica, A., and A. Mantovani. 2012. Macrophage plasticity and polarization: in vivo veritas. *J. Clin. Invest.* 122:787–795. http://dx.doi.org/10.1172/JCI59643

Smith, S.C., and P.M. Allen. 1991. Myosin-induced acute myocarditis is a T cell-mediated disease. *J. Immunol.* 147:2141–2147.

Smith, S.C., and P.M. Allen. 1993. The role of T cells in myosin-induced autoimmune myocarditis. *Clin. Immunol. Immunopathol.* 68:100–106. http://dx.doi.org/10.1006/clin.1993.1103

Swirski, F.K.F.K., M. Nahrendorf, M. Etzrodt, M. Wildgruber, V. Cortez-Retamozo, P. Panizzi, J.L.J.-L. Figueiredo, R.H.R.H. Kohler, A. Chudnovskiy, P. Waterman, et al. 2009. Identification of splenic reservoir monocytes and their deployment to inflammatory sites. *Science.* 325:612–616. http://dx.doi.org/10.1126/science.1175202

van Rooijen, N., A. Sanders, and T.K. van den Berg. 1996. Apoptosis of macrophages induced by liposome-mediated intracellular delivery of clodronate and propamidine. *J. Immunol. Methods.* 193:93–99. http://dx.doi.org/10.1016/0022-1759(96)00056-7

Vinten-Johansen, J. 2004. Involvement of neutrophils in the pathogenesis of lethal myocardial reperfusion injury. *Cardiovasc. Res.* 61:481–497. http://dx.doi.org/10.1016/j.cardiores.2003.10.011

Wantha, S., J.-E. Alard, R.T. Megens, A.M. van der Does, Y. Döring, M. Drechsler, C.T.N. Pham, M.-W. Wang, J.-M. Wang, R.L. Gallo, et al. 2013. Neutrophil-derived cathelicidin promotes adhesion of classical monocytes. *Circ. Res.* 112:792–801. http://dx.doi.org/10.1161/CIRCRESAHA.112.300666

Wilson, M.S., S.K. Madala, T.R. Ramalingam, B.R. Gochuico, I.O. Rosas, A.W. Cheever, and T.A. Wynn. 2010. Bleomycin and IL-1β-mediated pulmonary fibrosis is IL-17A dependent. *J. Exp. Med.* 207:535–552. http://dx.doi.org/10.1084/jem.20092121

Wynn, T.A., A. Chawla, and J.W. Pollard. 2013. Macrophage biology in development, homeostasis and disease. *Nature.* 496:445–455. http://dx.doi.org/10.1038/nature12034

Yona, S., K.-W. Kim, Y. Wolf, A. Mildner, D. Varol, M. Breker, D. Strauss-Ayali, S. Viukov, M. Guilliams, A. Misharin, et al. 2013. Fate mapping reveals origins and dynamics of monocytes and tissue macrophages under homeostasis. *Immunity.* 38:79–91. http://dx.doi.org/10.1016/j.immuni.2012.12.001

Yu, J.J., M.J. Ruddy, H.R. Conti, K. Boonanantanasarn, and S.L. Gaffen. 2008. The interleukin-17 receptor plays a gender-dependent role in host protection against *Porphyromonas gingivalis*-induced periodontal bone loss. *Infect. Immun.* 76:4206–4213. http://dx.doi.org/10.1128/IAI.01209-07

Yuan, J., A.-L. Cao, M. Yu, Q.-W. Lin, X. Yu, J.-H. Zhang, M. Wang, H.-P. Guo, and Y.-H. Liao. 2010. Th17 cells facilitate the humoral immune response in patients with acute viral myocarditis. *J. Clin. Immunol.* 30:226–234. http://dx.doi.org/10.1007/s10875-009-9355-z

Zbinden, S., R. Zbinden, P. Meier, S. Windecker, and C. Seiler. 2005. Safety and efficacy of subcutaneous-only granulocyte-macrophage colony-stimulating factor for collateral growth promotion in patients with coronary artery disease. *J. Am. Coll. Cardiol.* 46:1636–1642. http://dx.doi.org/10.1016/j.jacc.2005.01.068